Molecular Pharmacology Fast Forward. Published on June 25, 2020 as DOI: 10.1124/mol.120.119982
This article has not been copyedited and formatted. The final version may differ from this version.

Interaction of MDIMP with the voltage-gated calcium channels

Juan A. M. De La Rosa, Maricela García-Castañeda, Takuya Nishigaki, Juan Carlos Gómora,

Teresa Mancilla-Percino, and Guillermo Ávila

Departamento de Bioquímica, Cinvestav-IPN (JAMD, MGC, GA)

Departamento de Química, Cinvestav-IPN (TMP)

Instituto de Biotecnología, Universidad Nacional Autónoma de México (TN)

Instituto de Fisiología Celular, Universidad Nacional Autónoma de México (JCG)

Molecular Pharmacology Fast Forward. Published on June 25, 2020 as DOI: 10.1124/mol.120.119982
This article has not been copyedited and formatted. The final version may differ from this version.

Running Title: MDIMP, a novel calcium channel antagonist

Corresponding autor: Guillermo Ávila, Ph.D.

E-mail address: gavila@cinvestav.mx

Tel.: (+52) (55) 5747-3952

Fax: (+55) (55) 5747-3391

Departamento de Bioquímica, Cinvestav-IPN.

AP 14-740, México City, DF 07000, México.

Number of:

Tables. 1

Figures. 11

References. 36

Number of words in:

Abstract. 226

Introduction. 551

Discussion. 2187

Abbreviations: HVA, high voltage-activated; LVA, low voltage-activated; MDIMP, methyl (S)-2-(1,3-dihydroisoindol-2-yl)-4-methylpentanoate; VDCCs, voltage-dependent calcium channels.

Molecular Pharmacology Fast Forward. Published on June 25, 2020 as DOI: 10.1124/mol.120.119982
This article has not been copyedited and formatted. The final version may differ from this version.

ABSTRACT

Amino acid-derived isoindolines are synthetic compounds that were created with the idea of investigating their biological actions. The amino acid moiety was included on the grounds that it may help to avoid toxic effects. Recently, the isoindoline MDIMP was shown to inhibit both cardiac excitation-contraction coupling and voltage-dependent calcium channels (VDCCs). Here, we revealed that MDIMP binds preferentially to low voltage-activated (LVA) channels. Using a holding potential of -90 mV, the following IC_{50} values were found (in μM): >1000 ($Ca_V2.3$), 957 ($Ca_V1.3$), 656 ($Ca_V1.2$), 219 ($Ca_V3.2$), and 132 ($Ca_V3.1$). Moreover, the isoindoline also promoted both accelerated inactivation kinetics of HVA Ca^{2+} channels and a modest upregulation of $Ca_V1.3$ and $Ca_V2.3$. Additional data indicate that while MDIMP binds to the closed state of the channels, it has more preference for the inactivated one. Concerning $Ca_V3.1$, the compound did not alter the shape of the instantaneous I-V curve and substituting one or two residues in the selectivity filter drastically increased the IC_{50} value, suggesting that MDIMP binds to the extracellular side of the pore. However, an outward current failed in removing the inhibition, which implies an alternative mechanism may be involved. The enantiomer D-MDIMP, on the other hand, was synthesized and evaluated, but it did not improve the affinity to LVA channels. Implications of these findings are discussed in terms of the possible underlying mechanisms and pharmacological relevance.

Significance Statement.

We have studied the regulation of VGCCs by MDIMP, which disrupts excitation-contraction coupling in cardiac myocytes. The latter effect is more potent in atrial than ventricular myocytes, and this could be explained by our results showing that MDIMP preferentially blocks low voltage-activated (LVA) channels. Our data also provide mechanistic insights about the blockade and suggest that MDIMP is a promising member of the family of Ca^{2+} channel blockers, with possible application to the inhibition of subthreshold membrane depolarizations.

Molecular Pharmacology Fast Forward. Published on June 25, 2020 as DOI: 10.1124/mol.120.119982
This article has not been copyedited and formatted. The final version may differ from this version.

INTRODUCTION

Voltage-dependent ion channels are proteins found in most cells of an organism and are responsible for regulating rapid ion transport across the plasma membrane (Terlau and Stühmer, 1998). In particular, voltage-gated Ca^{2+} channels (VGCCs) allow the entry of this second messenger and thereby influence several cellular processes. The VGCCs can be classified as low and high voltage-activated (LVA and HVA), as well as of type L, N, P/Q, R, and T. Interestingly, LVA and HVA channels differ in the residues providing electronegativity to the four homologous domains of their selectivity filter. The former contains two glutamates and two aspartates (EEDD), whereas the latter has four glutamates (EEEE; Catterall, 2011). The L-type channels are sensitive to low concentrations (< 10 μM) of dihydropyridines (DHPs; Hess *et al.*, 1984), and each cell-type possesses its kit of channels. The case of VGCCs of atrial and ventricular myocytes is typical. In adult rat, for example, the former expresses both HVA ($Ca_V1.2$, $Ca_V1.3$, $Ca_V2.3$) and LVA ($Ca_V3.1$ and $Ca_V3.2$) channels, while the latter primordially expresses $Ca_V1.2$ (Piedras-Rentería *et al.*, 1997; Larsen *et al.*, 2002; Perez-Reyes, 2003; Zhang *et al.*, 2005; Zamponi *et al.*, 2015; Ríos-Pérez *et al.*, 2016).

The isoindolines are heterocyclic compounds consisting of a six-membered benzene ring fused to a five-membered ring containing a nitrogen atom at position two (Speck and Magauer, 2013). Molecular docking studies suggest that some of these compounds (isoindolines 2-substituted derivatives from α-amino acids) could bind to an L-type Ca^{2+} channel ($Ca_V1.2$). In particular, both the isoindoline MDIMP (also known as 1b) and a DHP antagonist showed similar binding profiles for $Ca_V1.2$. Moreover, the *in-silico* model also predicts that MDIMP binds to segments S5, S6, and loop P (of domain II), by interacting with residue F763 (S6) and the glutamate of the selectivity filter (E736; Mancilla-Percino *et al.*, 2010).

A previous work challenged the possibility that MDIMP regulates VGCCs in cardiac myocytes. Remarkably, the compound reduced the magnitude of both LVA and HVA calcium currents, acting more potently on the former. Additionally, MDIMP inhibited excitation-contraction (EC) coupling in both atrial and ventricular myocytes (Santamaria-Herrera *et al.*, 2016). This demonstrates that the isoindolines effectively target VGCCs, and thereby also impair EC coupling.

Here, we have investigated whether MDIMP selectively blocks a specific type of Ca^{2+} channel, using heterologous expression systems. Indeed, our results show that MDIMP acts preferentially on $Ca_V3.1$ and $Ca_V3.2$ (LVA

Molecular Pharmacology Fast Forward. Published on June 25, 2020 as DOI: 10.1124/mol.120.119982
This article has not been copyedited and formatted. The final version may differ from this version.

channels). Additional findings suggest that the occupancy of the binding site is state-dependent: the inactivated state enhances the affinity, and the site is also partially available in the closed configuration. We also describe experimental conditions that allow MDIMP to partially discriminate between two L-type calcium channels, $Ca_V1.2$ and $Ca_V1.3$. The effect on $Ca_V3.1$ channels was further characterized, and results from two mutations in the selectivity filter of this channel (DEDD and DDDD) suggest that this region might be important for the interaction (the potency of the blockade is reduced by 3- and 5-fold). Interestingly, however, we observed a similar percentage of inhibition on inward and outward currents, indicating that imposing a driving force for the efflux of ions does not unplug the ion-conducting pathway. Finally, MDIMP did not alter the shape of the instantaneous I-V curve, suggesting that the effect on a particular channel is all-or-none.

A preliminary report was presented recently (De La Rosa *et al.*, 2019).

MATERIALS AND METHODS.

Cell culture and transfection.

Human embryonic kidney (HEK) 293T/17 cells, a subclone of the HEK293 cell line, were acquired from the American Type Cell Culture Collection (ATCC, CRL-11268) and were grown and transfected as described previously (Santamaria-Herrera *et al.*, 2016). The following cDNAs (GenBank accession number included) were used: $Ca_V1.2$ (AY728090), $Ca_V1.3$ (AF370009), $Ca_V2.3$ (X67856), $ß_{2a}$ (M80545) and $\alpha_2\delta$-1 (M21948). The transfection mix consisted of equimolar amounts of cDNA encoding for one principal channel subunit, both accessory subunits and EGFP (as a reporter gene). In another set of experiments, 293T/17 cells were transfected with cDNAs encoding EGFP and mutant proteins of $Ca_V3.1$ (either DEDD or DDDD; Garza-López *et al.*, 2016). FuGENE® HD (Promega; Madison WI, USA) was used as a transfection reagent, according to the provider's instructions. All recordings were performed 48-72 h post-transfection, in green fluorescent cells. The activity of wild-type LVA channels ($Ca_V3.1$–AF190860 and $Ca_V3.2$–AF051946) was also investigated, in HEK293 cells stably transfected with the corresponding cDNAs (Díaz *et al.*, 2005; Lopez-Charcas *et al.*, 2012).

Molecular Pharmacology Fast Forward. Published on June 25, 2020 as DOI: 10.1124/mol.120.119982
This article has not been copyedited and formatted. The final version may differ from this version.

Voltage-clamp experiments.

Calcium currents (I_{Ca}) were recorded using the whole-cell patch-clamp technique, as described elsewhere (Santamaria-Herrera *et al.*, 2016). Unless otherwise specified, the holding potential (HP) was -90 mV. The whole-cell series resistance (R_s) and cell capacitance (C_m) were estimated using the capacitance cancellation feature of the amplifier (Axopatch 200B, Molecular Devices, LLC; San Jose, CA USA), and other linear components of the current signal were digitally eliminated (with a P/N leak subtraction protocol). R_s was electronically compensated (by 60 % to 70 %), and its final values were typically 1-2 MΩ. I_{Ca} was analogically filtered (at either 2 kHz or 10 kHz, using the 4-pole low pass Bessel filter of the amplifier, digitalized by an analogical to digital converter (Digidata 1322, Molecular Devices, LLC), and stored for off-line analysis. I_{Ca} was assessed before, during and after bathing the cells with MDIMP, its enantiomer (D-MDIMP), or the vehicle (DMSO).

In general, I_{Ca} was elicited by voltage steps delivered every 15 s, from the HP to either -20 mV (LVA channels) or +20 mV (HVA channels). For each particular cell, I_{Ca} values were normalized to those observed at ~105 s after break-in into the whole-cell mode, and at that time, MDIMP was applied, typically in two consecutive concentrations, followed by wash-out. In some cells, the behavior of I_{Ca} was assessed in the presence of only the control external solution (here termed “basal” I_{Ca}). To estimate the percentage of MDIMP effect, the I_{Ca} values observed in the presence of the compound were normalized to those of time-matched basal. Unless specified otherwise, the concentration-response curves were built from peak values of current traces and fitted according to the following Hill equation:

$$I_{Ca} = 100 /(1+[MDIMP]/ IC_{50})\exp(n_H)) \quad (1)$$

where I_{Ca} represents the percentage of inhibition, [MDIMP] is the MDIMP concentration, IC_{50} is the [MDIMP] required to 50% of the effect, and n_H is the Hill coefficient.

To investigate the steady-state voltage-dependence of inactivation, 5-s conditioning pulses to different potentials preceded a test pulse to -20 or +20 mV (LVA and HVA channels, respectively). Subsequently, the relative values of I_{Ca} were plotted as a function of membrane potential during pre-pulses, and the resulting inactivation curves were fitted according to the following Boltzmann equation:

$$I_{Ca} = I_{max}/ (1+\exp[-(V_m-V_{1/2})/k]) \quad (2)$$

Molecular Pharmacology Fast Forward. Published on June 25, 2020 as DOI: 10.1124/mol.120.119982
This article has not been copyedited and formatted. The final version may differ from this version.

where I_{max} represents the maximum current recruited at very negative potentials, $V_{1/2}$ is the potential required to reach 50 % of inactivation, and k is the slope factor.

Finally, the voltage-dependence of activation was assessed by fitting current-voltage curves (I-V curves) to the following Boltzmann equation:

$$I_{Ca} = G_{max} (V_m - V_{rev})/(1+\exp[(V_m - V_{1/2}))/k]) \quad (3)$$

where G_{max} is the maximal conductance, V_m is the membrane potential, V_{rev} represents the apparent reversal potential, $V_{1/2}$ is the membrane potential required to activate 50% of G_{max}, and k is the slope factor.

Recording solutions.

Unless otherwise specified, cells were bathed in an external solution containing (in mM): 10 $CaCl_2$, 150 tetraethylammonium chloride, 10 HEPES and 10 glucose (pH 7.3). Besides, the internal (pipette) solution contained (in mM): 140 Cs-Asp, 10 Cs-EGTA, 10 CsCl, 2 $CaCl_2$, 5 Mg-ATP, 0.05 Tris-GTP, 5 glucose and 10 HEPES (pH 7.3).

Stock solutions (100 mM) of MDIMP and its enantiomer (D-MDIMP) were prepared using DMSO as the solvent and then diluted in the external recording solution for obtaining final working concentrations. When high molarities of the compounds (i.e., 0.5-1 mM) were used, the external solution was warmed to avoid precipitation (10 min, ~50^o C; in a water bath). Indeed, concentrations higher than one mM were not investigated because of MDIMP tends to precipitate beyond this concentration. New working solutions were prepared daily, and direct exposure to light was avoided (though we do not know if MDIMP is light sensitive). The exchange of external solutions was performed by a fast perfusion system (SF-77B, Warner Instruments, LLC; Hamden, CT USA) that was digitally controlled. For all channels types, the vehicle alone (DMSO) was tested at concentrations where its mixture with MDIMP elicited a drastic reduction on I_{Ca}, and the solvent per se failed in producing significant changes.

Synthesis of D-MDIMP.

The strategy for synthesizing the new enantiomer D-MDIMP is illustrated as auxiliary material (Supplemental Figure 1), briefly: ***i***) The D-leucine methyl ester hydrochloride was prepared from D-leucine and trimethylsilyl chloride (TMSCl) in methanol according to the method described elsewhere (Li and Sha, 2008). ***ii***) Then, the new D-MDIMP was obtained from the reaction of D-leucine methyl ester hydrochloride, α,α'-dibromo-o-xylene and

Molecular Pharmacology Fast Forward. Published on June 25, 2020 as DOI: 10.1124/mol.120.119982
This article has not been copyedited and formatted. The final version may differ from this version.

$KHCO_3$ in acetonitrile, following the same strategy as for MDIMP (Mancilla-Percino *et al.*, 2001). The structure of D-MDIMP was characterized by ^{1}H and ^{13}C NMR and high-resolution mass spectrum (HRMS) (see figure S–1 for further details).

Statistical analysis. All data are presented as mean ± SD and were analyzed and plotted with the combined use of software suites: p-CLAMP (v.10.2, Molecular Devices) and SigmaPlot (v.12.3, Systat Software Inc; San Jose, CA. USA). Statistical significance was evaluated using two-tailed paired Student´s t-tests. All experiments were performed at room temperature (22-24 °C).

RESULTS

Our main aim was to investigate the effects of MDIMP on cardiac VGCCs expressed in heterologous systems. This experimental approach guarantees the identity of each particular channel and thus contributes to a better understanding of the underlying mechanisms. We began using an HP of -90 mV, which keeps most of the channels in the closed state.

In addition, we initially focused on the L-type Ca^{2+} channels $Ca_V1.3$ (Figs. 1A-1D) and $Ca_V1.2$. (Fig. 1, E-F). For each channel type, the basal levels of I_{Ca} were estimated under control conditions; that is, the behavior of I_{Ca} was studied as a function of time and in the absence of MDIMP. Figure 1A (*open circles*) provides an example of such basal behavior. It can be seen that the basal I_{Ca} of $Ca_V1.3$ decreases steadily within the next 10 min after having initiated the recordings (to an ~85 % of its initial magnitude). Another pool of cells was consecutively exposed to 750 µM and 1000 µM of MDIMP, and this promoted that the initial magnitude of I_{Ca} decreased to a higher percentage, compared with the basal (Fig. 1A, *green triangles*). MDIMP was then washed out, and the I_{Ca} slightly recovered from inhibition (Fig. 1A, *open triangles*). Results obtained from cells exposed to the compound were then divided by their time-matched basal, to only focus on MDIMP effects (which applies to all subsequent data). This analysis revealed that 750 µM and 1000 µM of MDIMP reduce the magnitude of I_{Ca} by ~20 % and ~40 %, respectively (Fig. 1B).

With additional data, a concentration-repose curve was built (Fig. 1C), and the following values of IC_{50} and Hill coefficient were obtained: 957 µM, and 3.5 (these parameters are also shown in Supplemental Table 1, together with those obtained for all channels types and experimental conditions). Of note, a low MDIMP concentration (250 µM)

Molecular Pharmacology Fast Forward. Published on June 25, 2020 as DOI: 10.1124/mol.120.119982
This article has not been copyedited and formatted. The final version may differ from this version.

promoted a slight increase in the activity of the $Ca_V1.3$ channel (see representative traces of Fig. 1D). As a result of this effect, the concentration-response curve showed a small but significant deviation toward negative values (of ~20 %, Fig. 1C). Thus, in the presence of MDIMP, the I_{Ca} of $Ca_V1.3$ likely reflects a balance between degrees of stimulation and inhibition.

Figure 1 also shows a summary of MDIMP effects on $Ca_V1.2$ (panels E and F). The corresponding IC_{50} was 656 µM, which is higher than a value previously reported (452 µM; Santamaria-Herrera *et al.*, 2016). This apparent inconsistency is likely due to an essential methodological difference: in the previous study, a depolarized HP of -50 mV was used. Below, we will come back to this point.

Next, we focused on $Ca_V2.3$, an HVA R-type Ca^{2+} channel (Fig. 2). In comparison with results from L-type Ca^{2+} channels (Fig. 1), MDIMP did not reduce the peak I_{Ca} of $Ca_V2.3$, even at the highest concentration tested (i.e., 1 mM). Nevertheless, the kinetics of I_{Ca} revealed a fascinating aspect: the rate of inactivation was drastically accelerated, in a concentration-dependent manner (Fig. 2, inset). Accordingly, the compound exerted a marked inhibition at the end of the test pulse (i.e., 200 ms), with an IC_{50} of 717 µM (Supplemental Figure 2).

Indeed, a similar effect on the inactivation rate of L-type Ca^{2+} channels was also observed (see, for example, the representative traces of Fig 1 and those of Santamaria-Herrera *et al.*, 2016). Moreover, by analyzing the I_{Ca} remaining at the end of the test pulse, the IC_{50} values obtained from the data in Fig. 1 were smaller than those estimated from the peak I_{Ca}. Specifically, they go from 957 µM to 290 µM ($Ca_V1.3$) and from 656 µM to <250 µM ($Ca_V1.2$; Supplemental Figure 2). The kinetics of inactivation was also studied by fitting exponential equations to the decaying phase of the current. In the case of $Ca_V1.3$, a second-order exponential was necessary, while a first-order exponential sufficed in both $Ca_V1.2$ and $Ca_V2.3$. In general, MDIMP reduced the value of time constants by ~50-60 % (except for a fast component of ~10 ms in $Ca_V1.3$, which was not altered; Supplemental Figure 3). Thus, MDIMP accelerates the rate of inactivation in all HVA Ca^{2+} channels, in spite that this process arises from distinct levels of complexity among channel subtypes.

Previous work in atrial myocytes showed that MDIMP preferentially inhibits LVA Ca^{2+} currents (I_{CaLVA}), suggesting a selective effect on Ca_V3 channels (Santamaria-Herrera *et al.*, 2016). In that work, however, this effect was not pursued further, because the amplitude of cardiac I_{CaLVA} is minimal (~30 pA). Thus, here we aimed to investigate whether MDIMP effectively inhibits LVA Ca^{2+} channels, with a higher potency than that observed for HVA

Molecular Pharmacology Fast Forward. Published on June 25, 2020 as DOI: 10.1124/mol.120.119982
This article has not been copyedited and formatted. The final version may differ from this version.

channels. Figure 3A shows examples of I_{Ca} that were obtained for $Ca_V3.2$, in the absence and presence of MDIMP (250 µM and 500 µM). The time course of average I_{Ca} values is also shown in Fig. 3B. It can be observed that MDIMP rapidly down-regulates $Ca_V3.2$, in approximately 30 s. Notably, 250 µM and 500 µM of MDIMP exert an inhibition of ~45 % and ~80 %, respectively. Thus, after analyzing the entire concentration-response curve, it was possible to conclude that MDIMP inhibits $Ca_V3.2$ with an IC_{50} of ~220 µM, corroborating the idea that MDIMP preferentially acts on Ca_V3 channels. This conclusion was further supported by results obtained for $Ca_V3.1$, as this channel exhibited the highest sensibility to MDIMP (Fig. 4). For example, the percentages of inhibition were, approximately: 75 % and 95 %, for 250 µM and 500 µM. Accordingly, the IC_{50} was ~130 µM (the lowest among all Ca^{2+} channel types that we have investigated).

It is also worth noting that MDIMP did not promote changes in the kinetic properties of Ca_V3 channels (Figs. 3A and 4A, see also Supplemental Figure 4), which is in striking contrast with results obtained from HVA Ca^{2+} channels. In the latter, the time course of inactivation was drastically accelerated (as described above and also shown in representative traces of Figs. 1A & 2A). Thus, MDIMP promotes "inactivation" but only in those channels exhibiting slow inactivation (i.e., HVA channels).

It is well-known that many drugs exert their effects depending on conformational states of the channels, and thus their modulatory actions depend indirectly on V_m. In the next section, therefore, we investigated the voltage-dependence of inactivation of Ca^{2+} channels, in the presence and absence of MDIMP. The corresponding data are shown summarized, in Fig. 5 & Table 1. In all channel types, the isoindoline shifted the steady-state inactivation curve toward more negative membrane potentials, suggesting that the inactivated state facilitates MDIMP binding or vice versa. The extent of this effect, however, is somewhat variable. More specifically, the shift in $V_{1/2}$ values is close to -20 mV, for both T- ($Ca_V3.1$, $Ca_V3.2$) and L-type Ca channels ($Ca_V1.2$ and $Ca_V1.3$), whereas $Ca_V2.3$ exhibits the most considerable shift (of approximately –40 mV; Fig. 5, Table 1). Indeed, the shape of inactivation curves was also significantly altered, but not in all types of channels. In particular, the k value was decreased for $Ca_V1.2$ and increased for both $Ca_V3.1$ and $Ca_V3.2$ (in all cases, the change in k was close to 5 mV; Fig. 5, Table 1).

In figure 6, the view that MDIMP preferentially binds to the inactivated state was further challenged, for HVA channels. In particular, the MDIMP effects were now assessed from an HP of -50 mV (a potential that allows transitions from closed to inactivated states, see figure 5). The corresponding IC_{50} values were (in µM): 445

Molecular Pharmacology Fast Forward. Published on June 25, 2020 as DOI: 10.1124/mol.120.119982
This article has not been copyedited and formatted. The final version may differ from this version.

($Ca_V1.2$), 231 ($Ca_V1.3$), and 557 ($Ca_V2.3$); that is, much smaller than those observed with an HP of -90 mV (compare data of Fig. 6A with those of Figs. 1 & 2). These data reinforce our conclusion that MDIMP preferentially binds to VGCCs in the inactivated state. Besides, similar to the observed with an HP of -90 mV, the IC_{50} values are also smaller if the I_{Ca} is assessed at the end of 200-ms pulses (Fig. 6B and inset).

Data showed in Fig. 6 suggest that an HP of -50 mV may help MDIMP to discriminate between $Ca_V1.2$ and $Ca_V1.3$ channels: the IC_{50} of the former nearly doubles that of the latter (Fig. 6). Thus, we decided to reexamine the effects of 250 μM MDIMP, on these two types of calcium channels, over an extended time scale (~10 min, as opposed to the typical 90-s applications). The data obtained from this experimental series are summarized in Fig. 7. In keeping with the results of Fig. 6A, 90 s of MDIMP application caused a notable inhibition of $Ca_V1.3$ (by approximately 60 %), while $Ca_V1.2$ was barely affected (~7 %). Moreover, although in both channel types the extent of inhibition continued growing, $Ca_V1.3$ showed the higher rate (τ=1.55 min, vs. τ=4.94 min), and by 10 min, the fraction of inhibition was: 0.93 ($Ca_V1.3$) and 0.43 ($Ca_V1.2$). Thus, 250 μM of MDIMP indeed helps to distinguish between $Ca_V1.2$ and $Ca_V1.3$.

We next wondered if MDIMP can also bind to the closed state of VGCCs, and this point was investigated for $Ca_V2.3$ (Fig. 8) and the two types of LVA channels (i.e., $Ca_V3.1$ and $Ca_V3.2$; Supplemental Figure 5). The experiment consisted in keeping the channels closed: that is, at an HP of -90 mV but exposed to MDIMP for a couple of minutes. Then, the percentage of effect on I_{Ca} was assessed at the first depolarizing pulse. In the case of $Ca_V2.3$, the action of the isoindoline was somewhat complex. A small increase in peak I_{Ca} (of 13 %) preceded a slight reduction in the magnitude of current remaining at 200 ms (of 21 %), and a striking change in current kinetics reflected these two effects (Fig. 8). Accordingly, the compound promoted a two-fold increase in the fraction of inactivation (i.e., from 0.25 ± 0.09 to 0.50 ± 0.10; P = 0.005). These data suggest that the closed state of the $Ca_V2.3$ HVA channel binds MDIMP, and this results in marked alterations in gating. Moreover, MDIMP also acts on the closed state of $Ca_V3.1$ and $Ca_V3.2$ channels, as evidenced by results from a similar protocol as in Fig.8, showing a significant reduction in the peak I_{Ca} (of 39 % and 26 %, respectively; Supplemental Figure 5). Thus, we conclude that the MDIMP binds to VGCCs not only in the inactivated (Fig. 5) state but also in the closed one.

We next focused on activation (or G-V) curves. In these experiments, the HVA Ca^{2+} channels were examined from an HP of -50 mV, to facilitate inhibition. As can be seen in Fig. 9, MDIMP promoted significant reductions on the

Molecular Pharmacology Fast Forward. Published on June 25, 2020 as DOI: 10.1124/mol.120.119982
This article has not been copyedited and formatted. The final version may differ from this version.

maximal conductance (G_{max}) of all channel types. In contrast, the slope factor (k) and midpoint ($V_{1/2}$) were in general unaltered: the only exception was for $Ca_V1.3$ and $Ca_V2.3$, whose $V_{1/2}$ values were shifted by nearly -4 mV (Fig. 9, Table 1).

Thus far, $Ca_V3.1$ is the channel with the highest affinity for MDIMP. This finding, combined with a previous suggestion that MDIMP binds to the selectivity filter of VGCCs (Mancilla-Percino *et al.*, 2010), motivated us to investigate whether substituting amino acids of the selectivity filter modifies the affinity for MDIMP. In particular, we studied the following point mutations: DEDD and DDDD (Garza-López *et al.*, 2016). The corresponding results are shown in Fig. 10A (representative traces) and Fig. 10B (concentration-response curves). It can be observed that MDIMP inhibited the activity of both mutant proteins, but the inhibition occurred at concentrations higher than those observed for the WT channel. For example, the mutant proteins were barely affected by 100 µM and 250 µM (Fig. 10), whereas these concentrations inhibited the WT channel by approximately 40 % and 80 % (Fig. 10, *dashed line*; see also Fig. 4). These results are in line with the view that the selectivity filter of VGCCs represents an important domain for MDIMP binding.

To obtain more insights about a possible pore-blocking mechanism, we decided to determine whether the ions flowing in the outward direction may unplug the $Ca_V3.1$ channel (by possible removing MDIMP from its putative binding site, in the selectivity filter). However, under our standard I_{Ca} recording conditions, depolarizations to 80 mV and 100 mV were unable to elicit a possible efflux of Cs^+ through $Ca_V3.1$. Therefore, we decided to study an outward Na^+ current instead, using a protocol described elsewhere (Fig. 11; Lopin *et al.*, 2012). The corresponding results indicate that this current is reduced to a ~50 % in the presence of 130 µM MDIMP (Figs. 11A and 11C). This effect is in agreement with the data of figures 4 and 9, in which the IC_{50} for I_{Ca} reduction was about 130 µM.

Moreover, MDIMP reduced to a similar extent the magnitude of both outward and inward (tail) currents, in the same pool of cells (Fig. 11C). The similarity of effects on inward and outward currents suggests that a driving force for the efflux of ions fails in releasing the MDIMP–$Ca_V3.1$ interaction. Unfortunately, this result does not support the pore-blocking hypothesis.

Figure 11 also shows instantaneous I-V curves that were obtained by analyzing the initial amplitude of the tail current (Figs. 11A and 11B). It can be observed that MDIMP did not alter the shape of the normalized curves (Fig. 11B, inset), indicating that the effect on a single channel is all-or-none (according to the terminology of Armstrong,

1971).

DISCUSSION

In this work, we studied the regulation of cardiac VGCCs by MDIMP, a novel inhibitor of both calcium channels and EC coupling, with atrial selectivity. Indeed, a previous study showed that MDIMP preferentially acts on LVA calcium currents of atrial myocytes, suggesting that Ca_V3 channels exhibit the highest affinity for this compound (Santamaria-Herrera *et al.*, 2016). In these cells, the LVA calcium current is thought to reflect the activity not only of Ca_V3 channels (i.e. $Ca_V3.1$ and $Ca_V3.2$) but also $Ca_V1.3$ and $Ca_V2.3$ (Piedras-Rentería *et al.*, 1997; Larsen *et al.*, 2002; Zhang *et al.*, 2005; Ríos-Pérez *et al.*, 2016). Thus, the present study represents the first unequivocal demonstration that MDIMP preferentially binds to Ca_V3 channels. In addition, our data suggest that the compound regulates these channels by acting in all-or-none fashion (for the instantaneous I-V curves have the same shape in the absence and presence of MDIMP).

Moreover, apart from describing the molecular and biophysical properties of the regulation, our study investigated the hypothesis that the selectivity filter represents the high-affinity receptor site for MDIMP. Indeed, evidence in favor of this view was obtained, as the mutations of the selectivity filter decreased the affinity for the compound. Nevertheless, the pore-blocking model could not be supported by analyzing effects on outward currents. Thus, further investigation is needed to establish more firmly the precise mechanism.

Below we discuss tentative mechanisms for the inhibition as well as the possible pharmacological and clinical relevance of MDIMP. From now on, the term “blockade” is used to indicate that MDIMP might bind within the selectivity filter of the channels. On the other hand, “modulation” (i.e., inhibition or stimulation), is reserved to imply that the MDIMP can bind to either, the pore, or an alternative site, resulting in allosteric consequences (i.e., alterations in gating).

Mechanisms of MDIMP effects on VGCCs.

The functional properties of a VGCC emerge from the movement of many segments, in at least one of the proteins that form the channel (i.e., main subunit). Thus, when a compound binds to an ion channel, it seems reasonable to expect that the function of the latter might be modified. The influence of the pore region, on functional properties, is not exempt from this principle. On the contrary, there are examples where pharmacological or molecular modifications of the pore result in significant functional effects. The pore blockade of Na^+ channels by Ca^{2+}, which

Molecular Pharmacology Fast Forward. Published on June 25, 2020 as DOI: 10.1124/mol.120.119982
This article has not been copyedited and formatted. The final version may differ from this version.

also shifts the open probability toward more positive potentials, is an emblematic example (Armstrong and Cota, 1991). Moreover, it was recently shown that substituting a single amino acid, located next to the glutamate that belongs to the selectivity filter of human $Ca_V1.2$ (located in domain II), eliminates Ca^{2+}-dependent inactivation—a process that begins intracellularly, with allosteric modulation (by Ca^{2+} and calmodulin) of the COOH-terminal domain (Abderemane-Ali *et al.*, 2019). Moreover, it has been reported that the point mutations of the selectivity filter significantly alter the gating of $Ca_V3.1$ (Talavera *et al.*, 2003). Thus, although the pore-blocking mechanism would seem to represent the most straightforward explanation to the finding that the potency of MDIMP varies with the selectivity filter configuration, it is also possible that, instead, the latter exerts a remote control on another binding site.

Currently, it is difficult to explain the apparent paradox that, under certain circumstances, a Ca^{2+} channel antagonist also elicits a significant increase in the activity of the channels. Something roughly similar has been reported for DHPs (e.g., Bean, 1985), and the explanation relies on using racemic mixtures and the well-known agonist and antagonist actions of DHP stereoisomers. In our study, however, this explanation can be ruled out, because the MDIMP was obtained from pure L-leucine. Indeed, we have also synthesized the D enantiomer (D-MDIMP, Supplemental Figure 1), to assess its potential to inhibit Ca_V3 channels. The results show that $Ca_V3.2$ exhibits roughly the same affinity for both MDIMP and D-MDIMP (Supplemental Figure 6). $Ca_V3.1$, on the other hand, showed a slightly lower sensitivity to D-MDIMP (i.e., the IC_{50} was ~260 µM, which is nearly 2-fold higher than that of MDIMP; Supplemental Figure 6). Accordingly, results from docking experiments indicate that the D-MDIMP has a lower affinity for the pore region of VGCCs, compared with MDIMP (data not shown).

Shifting the steady-state inactivation curve toward more negative potentials was a common feature of MDIMP effects. This can be interpreted to suggest that in all channels, the inactivated state facilitates binding of MDIMP, either to the pore or to an alternative site, and thereby the inactivation also promotes the corresponding blockade or inhibition. Preferential binding of drugs to the inactivated state is frequently observed. The example of DHPs, acting on Ca_V1 (L-type) channels is emblematic. For example, when the HP changes from -80 mV to -15 mV (i.e., from privileging the resting state to promoting inactivation), then the IC_{50} for the effect of nitrendipine dramatically decreases (up to ~2000-fold, from 730 nM to 0.36 nM; Bean, 1985). Another similitude between DHP antagonists and MDIMP is their ability to accelerate the inactivation rate of L-type Ca^{2+} channels (e.g., Bean, 1985; this study). Interestingly, it has been proposed that the DHPs bind to the lateral, lipid-facing side of the pore module, and this

Molecular Pharmacology Fast Forward. Published on June 25, 2020 as DOI: 10.1124/mol.120.119982
This article has not been copyedited and formatted. The final version may differ from this version.

promotes an allosteric modification (asymmetry) of ion binding sites, which in turn results in high-affinity Ca^{2+} binding and blockade of the selectivity filter (Tang *et al.*, 2016). Thus, it will be important for future studies to determine whether the MDIMP and DHPs share a common binding site in VGCCs (as suggested by a theoretical model; Mancilla-Percino *et al.*, 2010).

In contrast with the observation that in all types of VGCCs, the inactivated state facilitates the interaction with the isoindoline, some of our findings were somewhat channel-type specific. For example, the apparent inactivation rate was accelerated by MDIMP, but only in HVA channels. In theory, this effect could be explained by the following two possible mechanisms.

i) MDIMP binds to an alternative site, which results in a configuration that is primed to accelerate inactivation. This mechanism implies that MDIMP somehow modulates the particles (or segments) that provoke inactivation. According to our results, this site is partially available in the closed configuration (Fig. 8 & Supplemental Figure 5), and the inactivated state promotes its occupancy (Fig. 5), thereby creating a positive feedback loop.

ii) The open state facilitates the blockade. This possibility arises from assuming that the movement of activation gates, to the open position, liberates access to a binding site, located in the selectivity filter. A precedent exists for this mechanism regarding LVA channels and antiepileptic drugs (succinimides). More precisely, it has been reported that these drugs not only show a high affinity for the inactivated state but also accelerate the apparent inactivation rate of I_{CaLVA}. To investigate whether a possible pore-blocking mechanism explains these findings, Gomora et al. (2001) compared the percentage of effect on inward and outward currents and found that these compounds significantly alter the influx of Ca^{2+} but have little impact on outward currents (carried through $Ca_V3.3$). This unidirectional action was interpreted to suggests that succinimides indeed clog the pore. Moreover, it also indicates that the ions flowing in the outward direction unplug the channel (Gomora *et al.*, 2001).

In the present study, we did not observe an unplug of $Ca_V3.1$ channels, by the outward current, despite the view that MDIMP might bind to the selectivity filter. Thus, the identification of the actual binding site(s) warrants further investigation.

Currently, it is hard to understand why an outward current failed to release the supposed interaction of MDIMP with an outer pore domain. This apparent inconsistency could be explained by proposing that the interaction promotes a pore collapse. Under these circumstances, the intracellular ions would be trapped. That is, unable to pass through a

Molecular Pharmacology Fast Forward. Published on June 25, 2020 as DOI: 10.1124/mol.120.119982
This article has not been copyedited and formatted. The final version may differ from this version.

collapsed pore, which represents a physical barrier for reaching—and expulsing—MDIMP. Apart from serving as a conciliatory mechanism, this idea of "pore collapse" is consistent with our results suggesting that MDIMP acts in an all-or-none fashion (Fig. 11B).

Potential pharmacological and clinical significance of MDIMP.

The relevance of Ca_V3 channels for the cardiac function is related to peacemaker depolarization, and thereby their blockade is thought to be cardioprotective in the context of atrial fibrillation. Besides, they can be re-expressed under certain pathological conditions, as part of the neonatal program of gene expression. More generally, the Ca_V3 channels participate in regulating the function of a number of cell types, including not only excitable but also non-excitable cells (Perez-Reyes, 2003; Zamponi *et al.*, 2015). Thus, a selective blockade of Ca_V3 channels by MDIMP could be of therapeutic benefit. The finding that this compound preferentially inhibits EC coupling in atrial vs. ventricular myocytes, combined with the fact that Ca_V3 channels are only expressed in the former cells, indirectly supports this interpretation.

On the other hand, the affinity of Ca_V3 channels for MDIMP is not higher than that found for other compounds. Indeed, certain compounds exert their effects with IC_{50} values in the low micromolar range (Perez-Reyes, 2003; Hashimoto and Kawazu, 2015). However, apart from selectivity, the tolerability is also essential, for a compound to be clinically relevant. Therefore, it is crucial to keep in mind that an amino acid was included into MDIMP, with the idea of making a more tolerable compound on the grounds that adducts of amino acids are highly stable (Flückiger *et al.*, 1984; Mancilla-Percino *et al.*, 2010; Santamaria-Herrera *et al.*, 2016). Indeed, they give rise to less variety of species in solution (e.g., Hofer *et al.*, 2013). Thus, future research may lead to concluding that MDIMP is advantageous for in vivo conditions, possibly based on less adverse effects.

The calcium channels of sperm cells (CatSper) present the same pore motif as that of the $Ca_V3.1$ DDDD mutant protein (Navarro *et al.*, 2008). This similitude, combined with the finding that the DDDD mutation decreases the affinity of $Ca_V3.1$ for MDIMP strongly suggests that CatSper should also exhibit relatively low MDIMP affinity. Likewise, other HVA channels not investigated here (but expressing four glutamates, EEEE), are also expected to be MDIMP-resistant. $Ca_V3.3$, on the other hand, is expected to share the same high-affinity as $Ca_V3.1$ and $Ca_V3.2$. Further work is needed to test all these predictions.

In addition to VGCCs, other molecular targets likely mediate the biological activities of MDIMP. For example, it

Molecular Pharmacology Fast Forward. Published on June 25, 2020 as DOI: 10.1124/mol.120.119982
This article has not been copyedited and formatted. The final version may differ from this version.

has been shown that the isoindolines derived from α-amino acids exert antitumoral effects and also act as enzyme inhibitors (of COX-1, COX-2 & HDAC8). The corresponding IC_{50} values for MDIMP were, approximately (in mM): 3.2 (cell viability), 0.7 (COX-1), 1.4, (COX-2), and 0.2 (HDAC8) (Trejo-Muñoz *et al.*, 2013; Trejo-Muñoz *et al.*, 2014; Mancilla-Percino *et al.*, 2016). On the other hand, we found that depolarized membrane potentials enhance the affinity of MDIMP for VGCCs. Indeed, 130 μM of the compound inhibits $Ca_V3.1$ by ~90 % (instead of the 50 % that is observed at an HP of -90 mV). This indicates the presence of a use-dependent block that could be relevant in electrically active cells. Therefore, we speculate that blood levels as low as 30-40 μM (which, in theory, do not compromise cell viability) should be sufficient for reverting an exacerbated excitability in vivo. It is important to emphasize, however, that the therapeutic window of MDIMP has yet to be experimentally determined.

Independently of its potential to be used clinically, MDIMP may also be helpful to dissect the activity of non-T-type calcium channels in native expression systems. Specifically, in conditions where HVA channels exhibit characteristics typically associated with LVA channels. For example, in rat atrial myocytes, where the LVA calcium current is thought to reflect the activity of not only $Ca_V3.1$ and $Ca_V3.2$, but also $Ca_V1.3$ and $Ca_V2.3$ (Larsen *et al.*, 2002; Piedras-Rentería *et al.*, 1997; Zhang *et al.*, 2005; Ríos-Pérez *et al.*, 2016).

To date, a pharmacological tool that selectively targets $Ca_V1.3$ does not exist (Zamponi *et al.*, 2015). A pyrimidine-2,4,6-trione derivate (Cp8) was thought to represent a selective blocker because it seems to discriminate between $Ca_V1.2$ and $Ca_V1.3$ (Kang *et al.*, 2012). However, this observation was unconfirmed in more recent studies (Huang *et al.*, 2014; Ortner *et al.*, 2014). Moreover, one of them found that Cp8 instead stimulates the activity of both channel types (Ortner *et al.*, 2014). Our results suggesting that MDIMP could help to distinguish the activity of L-type Ca^{2+} channel subtypes in native cells (Fig. 7) is relevant in this context. Nevertheless, we believe that additional efforts are needed to find the most selective compound. MDIMP forms part of an extensive list of molecules termed amino acid-derived isoindolines (Mancilla-Percino *et al.*, 2001), whose biological activities remain practically unexplored. Thus, our ongoing work is focused on characterizing a possible regulation of VGCCs by other members of this family.

In conclusion, we have investigated the mechanisms and specificity of MDIMP effects on VGCCs. Our results indicate that this isoindoline preferentially binds to Ca_V3 channels, possibly in the selectivity filter, which in turn may be eliciting a collapse of the pore. In addition, our results suggest that MDIMP is useful to discriminate

between $Ca_V1.2$ and $Ca_V1.3$ (L-type) channels. The corresponding pharmacological relevance for the in vivo condition, as well as the possibility that other amino acid-derived isoindolines also regulate VGCCs have yet to be investigated.

ACKNOWLEDGMENTS

We thank Drs. Robert T. Dirksen and Ulises Meza for proving cDNA clones used in this study. We also thank Salvador Carrasco for technical assistance.

AUTHORSHIP CONTRIBUTIONS

Participated in research design: De La Rosa, and Ávila

Conducted experiments: De La Rosa, García-Castañeda, and Ávila

Contributed new reagents or analytic tools: Nishigaki, Gómora, and Mancilla-Percino

Performed data analysis: De La Rosa, and Ávila

Wrote or contributed to the writing of the manuscript: De La Rosa, and Ávila

Molecular Pharmacology Fast Forward. Published on June 25, 2020 as DOI: 10.1124/mol.120.119982
This article has not been copyedited and formatted. The final version may differ from this version.

REFERENCES

Abderemane-Ali F, Findeisen F, Rossen ND, and Minor DL (2019) A Selectivity Filter Gate Controls Voltage-Gated Calcium Channel Calcium-Dependent Inactivation. *Neuron* **101**:1134-1149.e3.

Armstrong CM (1971) Interaction of tetraethylammonium ion derivatives with the potassium channels of giant axons. *J Gen Physiol* **58**:413–437.

Armstrong CM, and Cota G (1991) Calcium ion as a cofactor in Na channel gating. *Proc Natl Acad Sci USA* **88**:6528–6531.

Bean BP (1985) Two kinds of calcium channels in canine atrial cells. Differences in kinetics, selectivity, and pharmacology. *J Gen Physiol* **86**:1–30.

Catterall WA (2011) Voltage-gated calcium channels. *Cold Spring Harb Perspect Biol* **3**:a003947.

De La Rosa JAM, García-Castañeda M, Nishigaki T, Carlos Gomora J, Mancilla-Percino T, and Avila G (2019) Pore-Blocking Effect of Isoindoline MDIMP on Voltage-Gated Calcium Channels. *Biophysical Journal* **116**:113a–114a.

Díaz D, Bartolo R, Delgadillo DM, Higueldo F, and Gomora JC (2005) Contrasting effects of Cd2+ and Co2+ on the blocking/unblocking of human Cav3 channels. *J Membr Biol* **207**:91–105.

Flückiger R, Henson E, Hess GM, and Gallop PM (1984) Mass spectral and HPLC analysis of biological compounds with diphenylborinic acid. *Biomed Mass Spectrom* **11**:611–615.

Garza-López E, Chávez JC, Santana-Calvo C, López-González I, and Nishigaki T (2016) Cd(2+) sensitivity and permeability of a low voltage-activated Ca(2+) channel with CatSper-like selectivity filter. *Cell Calcium* **60**:41–50.

Gomora JC, Daud AN, Weiergräber M, and Perez-Reyes E (2001) Block of cloned human T-type calcium channels by succinimide antiepileptic drugs. *Mol Pharmacol* **60**:1121–1132.

Hashimoto N, and Kawazu T (2015) Pharmacological Profiles of T-Type Calcium Channel Antagonists, in *T-type Calcium Channels in Basic and Clinical Science* (Schaffer SW, and Li M eds) pp 37–48, Springer Vienna.

Hess P, Lansman JB, and Tsien RW (1984) Different modes of Ca channel gating behaviour favoured by dihydropyridine Ca agonists and antagonists. *Nature* **311**:538–544.

Hofer A, Kovacs G, Zappatini A, Leuenberger M, Hediger MA, and Lochner M (2013) Design, synthesis and pharmacological characterization of analogs of 2-aminoethyl diphenylborinate (2-APB), a known store-operated calcium channel blocker, for inhibition of TRPV6-mediated calcium transport. *Bioorganic & Medicinal Chemistry* **21**:3202–3213.

Huang H, Ng CY, Yu D, Zhai J, Lam Y, and Soong TW (2014) Modest CaV1.342-selective inhibition by compound 8 is β-subunit dependent. *Nat Commun* **5**:4481.

Kang S, Cooper G, Dunne SF, Dusel B, Luan C-H, Surmeier DJ, and Silverman RB (2012) CaV1.3-selective L-type calcium channel antagonists as potential new therapeutics for Parkinson's disease. *Nat Commun* **3**:1146.

Larsen JK, Mitchell JW, and Best PM (2002) Quantitative analysis of the expression and distribution of calcium channel alpha 1 subunit mRNA in the atria and ventricles of the rat heart. *J Mol Cell Cardiol* **34**:519–532.

Li J, and Sha Y (2008) A convenient synthesis of amino acid methyl esters. *Molecules* **13**:1111–1119.

Lopez-Charcas O, Rivera M, and Gomora JC (2012) Block of human CaV3 channels by the diuretic amiloride. *Mol Pharmacol* **82**:658–667.

Lopin KV, Gray IP, Obejero-Paz CA, Thévenod F, and Jones SW (2012) Fe^{2+} block and permeation of CaV3.1 (α1G) T-type calcium channels: candidate mechanism for non-transferrin-mediated Fe^{2+} influx. *Mol Pharmacol* **82**:1194–1204.

Mancilla-Percino T, Carrillo L, Zamudio-Rivera LS, Beltrán HI, and Farfán N (2001) Synthesis and characterization of new 2-substituted isoindoline derivatives of α-amino acids. *Organic Preparations and Procedures International* **33**:341–349.

Mancilla-Percino T, Correa-Basurto J, Trujillo-Ferrara J, Ramos-Morales FR, Acosta Hernández ME, Cruz-Sánchez JS, and Saavedra-Vélez M (2010) Molecular modeling study of isoindolines as L-type Ca(2+) channel blockers by docking calculations. *J Mol Model* **16**:1377–1382.

Mancilla-Percino T, Trejo-Muñoz CR, Díaz-Gandarilla JA, Talamás-Rohana P, Guzmán Ramírez JE, Cervantes J, and Figueroa Ortíz A (2016) Isoindoline Derivatives of α-Amino Acids as Cyclooxygenase 1 and 2 Inhibitors. *Arch Pharm (Weinheim)* **349**:175–185.

Navarro B, Kirichok Y, Chung J-J, and Clapham DE (2008) Ion channels that control fertility in mammalian spermatozoa. *Int J Dev Biol* **52**:607–613.

Ortner NJ, Bock G, Vandael DHF, Mauersberger R, Draheim HJ, Gust R, Carbone E, Tuluc P, and Striessnig J (2014) Pyrimidine-2,4,6-triones are a new class of voltage-gated L-type Ca2+ channel activators. *Nat Commun* **5**:3897.

Perez-Reyes E (2003) Molecular physiology of low-voltage-activated t-type calcium channels. *Physiol Rev* **83**:117–161.

Piedras-Rentería ES, Chen CC, and Best PM (1997) Antisense oligonucleotides against rat brain alpha1E DNA and its atrial homologue decrease T-type calcium current in atrial myocytes. *Proc Natl Acad Sci USA* **94**:14936–14941.

Ríos-Pérez EB, García-Castañeda M, Monsalvo-Villegas A, and Avila G (2016) Chronic atrial ionic remodeling by aldosterone: potentiation of L-type Ca2+ channels and its arrhythmogenic significance. *Pflugers Arch* **468**:1823–1835.

Santamaria-Herrera MA, Ríos-Pérez EB, de la Rosa JAM, García-Castañeda M, Osornio-Garduño DS, Ramos-Mondragón R, Mancilla-Percino T, and Avila G (2016) MDIMP, a novel cardiac Ca(2+) channel blocker with atrial selectivity. *Eur J Pharmacol* **781**:218–228.

Speck K, and Magauer T (2013) The chemistry of isoindole natural products. *Beilstein J Org Chem* **9**:2048–2078.

Talavera K, Janssens A, Klugbauer N, Droogmans G, and Nilius B (2003) Pore structure influences gating properties of the T-type Ca2+ channel alpha1G. *J Gen Physiol* **121**:529–540.

Tang L, Gamal El-Din TM, Swanson TM, Pryde DC, Scheuer T, Zheng N, and Catterall WA (2016) Structural basis for inhibition of a voltage-gated Ca2+ channel by Ca2+ antagonist drugs. *Nature* **537**:117–121.

Terlau H, and Stühmer W (1998) Structure and function of voltage-gated ion channels. *Naturwissenschaften* **85**:437–444.

Trejo-Muñoz CR, Mancilla-Percino T, Mera-Jiménez E, Correa-Basurto J, and Trujillo-Ferrara JG (2013) Partition coefficient determination of a series of isoindolines-2-substituted and its correlation with their antiproliferative activity on HeLa cells. *Med Chem Res* **22**:4039–4045.

Trejo-Muñoz CR, Mera-Jiménez E, Pinto-Almazán R, Díaz-Gandarilla JA, Correa-Basurto J, Trujillo-Ferrara JG, Guerra-Araiza C, Talamás-Rohana P, and Mancilla-Percino T (2014) Effect of two series of isoindolines over HDAC8 activity and expression. *Med Chem Res* **23**:3227–3234.

Zamponi GW, Striessnig J, Koschak A, and Dolphin AC (2015) The Physiology, Pathology, and Pharmacology of Voltage-Gated Calcium Channels and Their Future Therapeutic Potential. *Pharmacol Rev* **67**:821–870.

Zhang Z, He Y, Tuteja D, Xu D, Timofeyev V, Zhang Q, Glatter KA, Xu Y, Shin H-S, Low R, and Chiamvimonvat N (2005) Functional roles of Cav1.3(alpha1D) calcium channels in atria: insights gained from gene-targeted null mutant mice. *Circulation* **112**:1936–1944.

FOOTNOTES

This work was supported by Consejo Nacional de Ciencia y Tecnologia [grant #253009 to GA].

Part of this work was presented at the Biophysical Society Annual Meeting. March 02-06, 2019; Baltimore, Maryland, USA.

Molecular Pharmacology Fast Forward. Published on June 25, 2020 as DOI: 10.1124/mol.120.119982
This article has not been copyedited and formatted. The final version may differ from this version.

LEGENDS FOR FIGURES

Figure 1. MDIMP effects on L-type Ca^{2+} channels. **A**) The open circles represent I_{Ca} of $Ca_V1.3$ that was recorded as a function of time, under control or basal conditions (n = 6). Another cell group (triangles, n = 3) was consecutively exposed to 750 µM and 1000 µM of MDIMP (green symbols) and then the compound was washed-out (open triangles). All results obtained from each particular cell were normalized by the absolute I_{Ca} value that was observed at min 1.75 (just before MDIMP application). **B**) Same data set shown as triangles in A but divided by the corresponding time-matched basal (A, circles). **C**) concentration-response curve built from data obtained as in B. 250 µM of MDIMP increased the peak magnitude of I_{Ca} (data point with negative values) and thus the curve was fitted according to a slightly modified version of equation 1. Specifically, a constant was added to account for the negative deviation (-20.2 %). **D**) Representative current traces obtained from $Ca_V1.3$-expressing cells, in the presence of distinct MDIMP concentrations (numbers, in µM). The currents were normalized to the peak value of the control (black trace). **E, F**) Concentration-response curve (E) and representative traces (F) obtained from $Ca_V1.2$-expressing cells (as in A-D). In both cases ($Ca_V1.3$ & $Ca_V1.2$) MDIMP accelerated the rate of I_{Ca} inactivation (D, F, Supplemental Figure 3).

Figure 2. Effects on $Ca_V2.3$ channels. Average values of peak I_{Ca} expressed as a percentage of inhibition by different concentrations of MDIMP. The inset shows examples of current traces carried by $Ca_V2.3$, which were used to obtain the concentration-response curve. Rather than being reduced, the peak I_{Ca} showed a tendency to be increased in response to MDIMP. Additionally, the compound promoted an acceleration on the kinetics of current decay (see also Supplemental Figure 3). The results were obtained and analyzed as in Fig. 1.

Figure 3. MDIMP effects on $Ca_V3.2$ channels. **A**) Representative traces of I_{Ca} that were recorded in a $Ca_V3.2$-expressing cell, in the absence (control), presence and wash-out of MDIMP (250 and 500 µM). **B**) Time course of average values of I_{Ca} (recorded as in A, n = 3). **C**) Concentration-response curve obtained from experiments as in A and B.

Figure 4. MDIMP effects on $Ca_V3.1$ channels. **A-C**) Recordings of I_{Ca} carried through $Ca_V3.1$ in the absence and presence of distinct molarities (µM) of MDIMP (**A**) and corresponding time course of inhibition (**B**) and concentration-response curve (**C**). Data were obtained as described in Fig. 3.

Molecular Pharmacology Fast Forward. Published on June 25, 2020 as DOI: 10.1124/mol.120.119982
This article has not been copyedited and formatted. The final version may differ from this version.

Figure 5. MDIMP shifts towards more negative potentials the voltage-dependence of inactivation. **A, B**) Representative current traces that were used to investigate the steady-state voltage-dependence of inactivation in the absence (Control) and presence of MDIMP. A 5-s prepulse to distinct membrane potentials (V_m) preceded test pulses to either +20 mV (**A**, HVA channels) or -20 mV (**B**, LVA channels). **C, D**) Average inactivation curves that were obtained from recordings as in A and B. The circles represent Control conditions, whereas colored symbols indicate the presence of MDIMP. For each data set, the peak I_{Ca} was normalized to its maximum value, plotted as a function of prepulse potential, and the resulting inactivation curves were fitted according to a Boltzmann equation (Eqn. 2). The corresponding parameters are given in Table 1, and their mean values were used to calculate the smooth lines. Results are from a total of four to five investigated cells (per channel type). The MDIMP concentration was (in µM): 130 ($Ca_V3.1$), 220 ($Ca_V3.2$), 500 ($Ca_V1.2$ and $Ca_V2.3$), and 1000 ($Ca_V1.3$).

Figure 6. A depolarized HP increases the sensitivity of HVA Ca^{2+} channels to MDIMP. **A**) Percentage of peak I_{Ca} inhibition as a function of MDIMP concentration. I_{Ca} was elicited as described in figures 1 and 2 but using a HP of -50 mV. **B**) Same data as in A, except that I_{Ca} was measured 200 ms after test pulse onset. **C**) Examples of current traces that were recorded in presence of distinct MDIMP concentrations (numbers, in µM) and then used to analyze the degrees of inhibition showed in A and B. The inset illustrates IC_{50} values that were obtained using either the peak magnitude of I_{Ca} or the current remaining at 200 ms.

Figure 7. MDIMP discriminates between $Ca_V1.2$ and $Ca_V1.3$. **A**) Normalized I_{Ca} values obtained from $Ca_V1.2$– and $Ca_V1.3$–expressing cells, in either absence (open symbols) or presence of 250 µM MDIMP (colored symbols). Test pulses (to + 20 mV) were applied from a HP of -50 mV, and data represent the mean ± SD from three cells per experimental condition. **B**) Examples of I_{Ca} traces that were analyzed to generate the results shown in A). The numbers indicate the time in presence of MDIMP (min).

Figure 8. MDIMP binds to the closed state of $Ca_V2.3$. **A**) Relative magnitude of I_{Ca} that was estimated both at its maximum level (peak, *squares*) and the end (200 ms, *triangles*) of test pulses, before (*1.75 min*) and 3.25 min after MDIMP exposure. During the MDIMP application, the membrane potential was kept at -90 mV (i.e., in absence of depolarizing test pulses). Then, a train of pulses was delivered (15 s cycle length), followed by the wash-out of MDIMP (I_{Ca} measurements are shown only for the 1st pulse of the train, *min 5*). $^aP = 0.011$, $^bP = 0.034$; compared with the corresponding control (1.75 min, n=5). **B**) Representative current traces that were used to generate data of

Molecular Pharmacology Fast Forward. Published on June 25, 2020 as DOI: 10.1124/mol.120.119982
This article has not been copyedited and formatted. The final version may differ from this version.

A.

Figure 9. MDIMP does not promotes major changes in the voltage dependence of Ca^{2+} channel activation. **A**) I-V curves obtained in the absence (gray symbols) and presence of MDIMP (closed symbols). The results were normalized to the maximum I_{Ca} value observed in each particular cell, in the absence of MDIMP. Subsequently, the I-V curves were fitted according to a Boltzmann equation (Eqn 3). The resulting parameters and number of experiments are given in Table 1. **B**) Activation curves that were estimated from the I_{Ca} values shown in A and their corresponding Boltzmann parameters. The values of Ca^{2+} conductance (G_{Ca}) were normalized to G_{max}. **C**) Examples of I_{Ca} families that were used to generate the data of A and B. The concentration of MDIM was (in µM): 500 ($Ca_V1.2$ and $Ca_V2.3$), 230 ($Ca_V1.3$), 220 ($Ca_V3.2$), and 130 ($Ca_V3.1$).

Figure 10. Mutations in the selectivity filter of $Ca_V3.1$ interfere with the affinity for MDIMP. **A**) Calcium currents carried through $Ca_V3.1$ mutant channels (DEDD and DDDD) in the presence of distinct MDIMP concentrations (µM). **B**) Concentration-response curves that were obtained from recordings as in A; the estimated IC_{50} values are 387 µM (DEDD) and 543 µM (DDDD). A dashed line representing data gathered for the wild-type $Ca_V3.1$ is shown for comparison (see figure 4).

Figure 11. An outward current cannot release the inhibition by MDIMP. **A**) Experimental protocol and representative traces of ionic current (I_m) used to compare MDIMP (130 µM) effects on inward and outward currents. **B**) Average values of I_m that were obtained from tail currents as those shown in A, as a function of V_m (instantaneous I-V curves). The inset shows the same I-V curves but after dividing every data set by its corresponding value observed at -120 mV. The decaying phase of tail currents was fitted to a single exponential equation, and I_m represents an extrapolation to the time of repolarization. No significant differences were found among experimental groups regarding time constants for current decay (closing kinetics). **C**) Percentages of I_m inhibition by MDIMP that were estimated at the indicated membrane potential. The results were obtained from five $Ca_V3.1$-expressing cells, using the following recording solutions (in mM): 2 $CaCl_2$, 128 NaCl, 5 ascorbic acid, 10 glucose, and 20 HEPES (external); and 2 $CaCl_2$, 1 $MgCl_2$, 120 NaCl, 10 HEPES, 4 MgATP, and 11 EGTA. In both cases, the pH was adjusted to 7.3 with NaOH.

Molecular Pharmacology Fast Forward. Published on June 25, 2020 as DOI: 10.1124/mol.120.119982
This article has not been copyedited and formatted. The final version may differ from this version.

TABLES

TABLE 1

Parameters of fitted Steady-state inactivation and I -V curves

		Steady-state Inactivation-V data			I-V data			
		$V_{1/2}$ (mV)	k (mV)	n	$V_{1/2}$ (mV)	k (mV)	V_{rev} (mV)	n
$Ca_V1.2$	CONTROL	-7.3 ± 5.4	11.0 ± 4.0	5	13.7 ± 4.3	7.7 ± 0.9	81.4 ± 5.0	8
	MDIMP	-28.3 ± 9.4 *	5.9 ± 1.8 *		12.9 ± 4.9	7.9 ± 0.8	77.9 ± 5.5	
$Ca_V1.3$	CONTROL	-25.3 ± 6.0	5.7 ± 1.7	5	4.4 ± 3.4	7.1 ± 0.7	71.8 ± 5.1	4
	MDIMP	-47.7 ± 9.9 *	6.9 ± 4.3		0.5 ± 3.4 *	6.7 ± 0.4	70.3 ± 6.1	
$Ca_V2.3$	CONTROL	-17.9 ± 9.1	12.2 ± 7.6	5	21.4 ± 4.2	7.0 ± 0.4	86.8 ± 8.6	7
	MDIMP	-59.7 ± 7.8 *	11.8 ± 3.4		17.2 ± 5.0 *	7.5 ± 0.9	85.7 ± 5.9	
$Ca_V3.1$	CONTROL	-46.9 ± 5.1	4.0 ± 0.6	4	-20.7 ± 4.5	5.3 ± 1.4	50.0 ± 6.9	4
	MDIMP	-66.6 ± 10.1 *	9.7 ± 2.2 *		-22.6 ± 2.4	5.1 ± 0.9	47.3 ± 12.0	
$Ca_V3.2$	CONTROL	-53.0 ± 2.8	6.0 ± 1.2	4	-23.4 ± 5.4	5.5 ± 1.8	55.7 ± 2.8	3
	MDIMP	-72.8 ± 4.6 *	9.9 ± 0.7 *		-25.8 ± 3.9	5.8 ± 1.2	57.2 ± 5.3	

* Compared to control, $P<0.05$

Molecular Pharmacology Fast Forward. Published on June 25, 2020 as DOI: 10.1124/mol.120.119982
This article has not been copyedited and formatted. The final version may differ from this version.

FIGURE 1

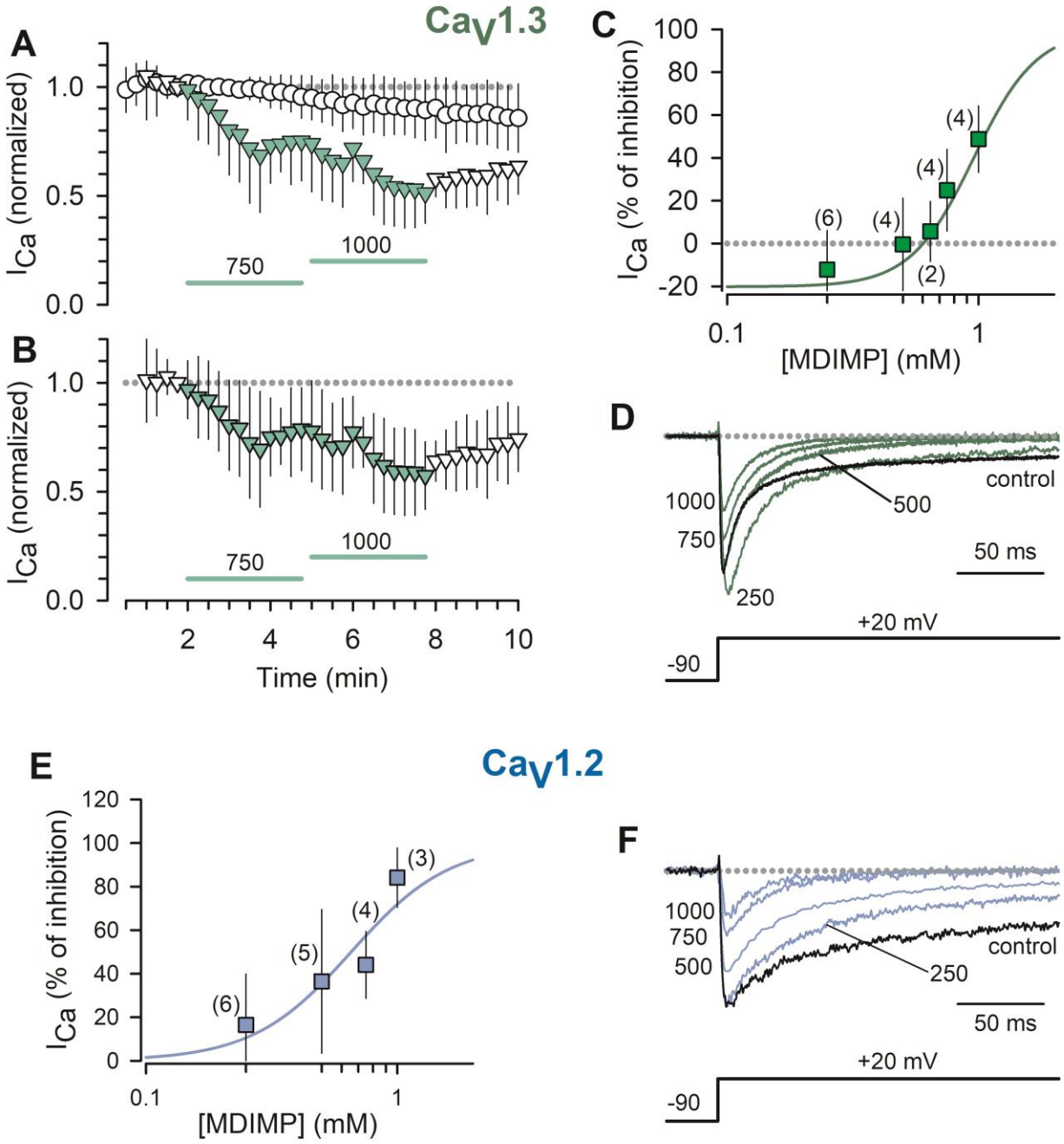

Molecular Pharmacology Fast Forward. Published on June 25, 2020 as DOI: 10.1124/mol.120.119982
This article has not been copyedited and formatted. The final version may differ from this version.

FIGURE 2

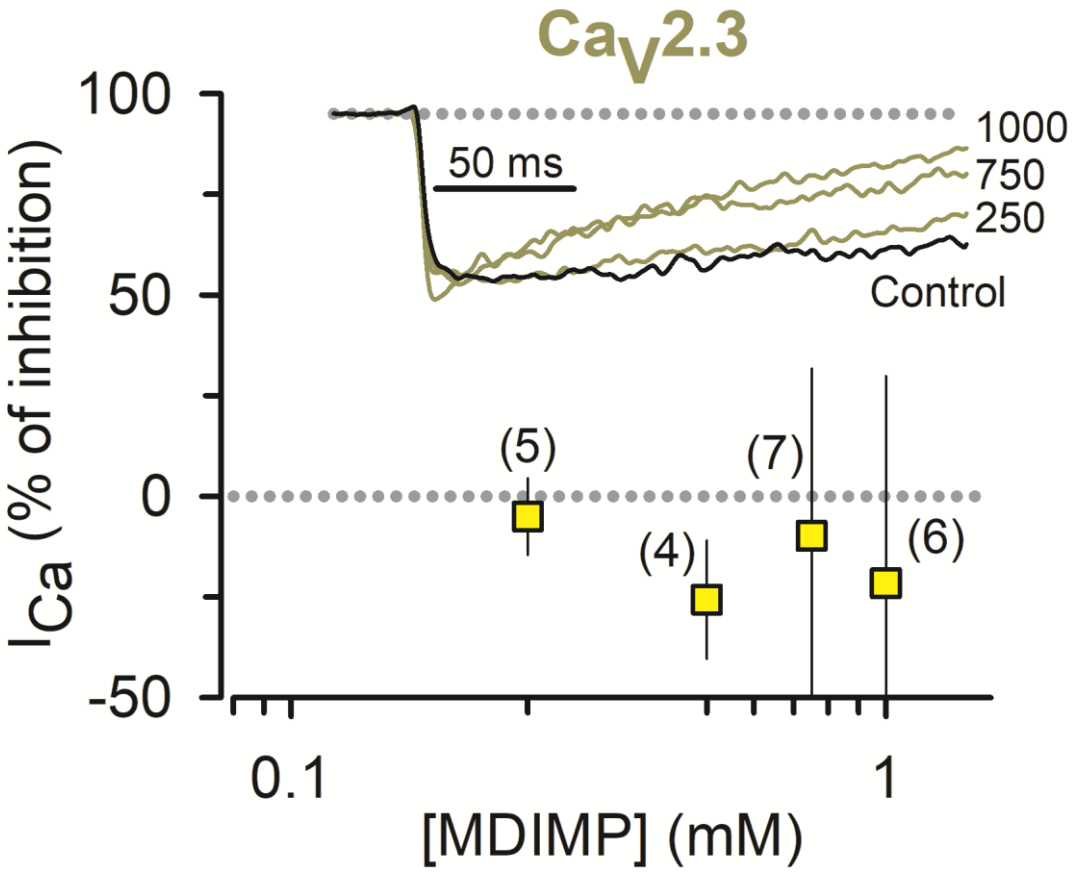

Molecular Pharmacology Fast Forward. Published on June 25, 2020 as DOI: 10.1124/mol.120.119982
This article has not been copyedited and formatted. The final version may differ from this version.

FIGURE 3

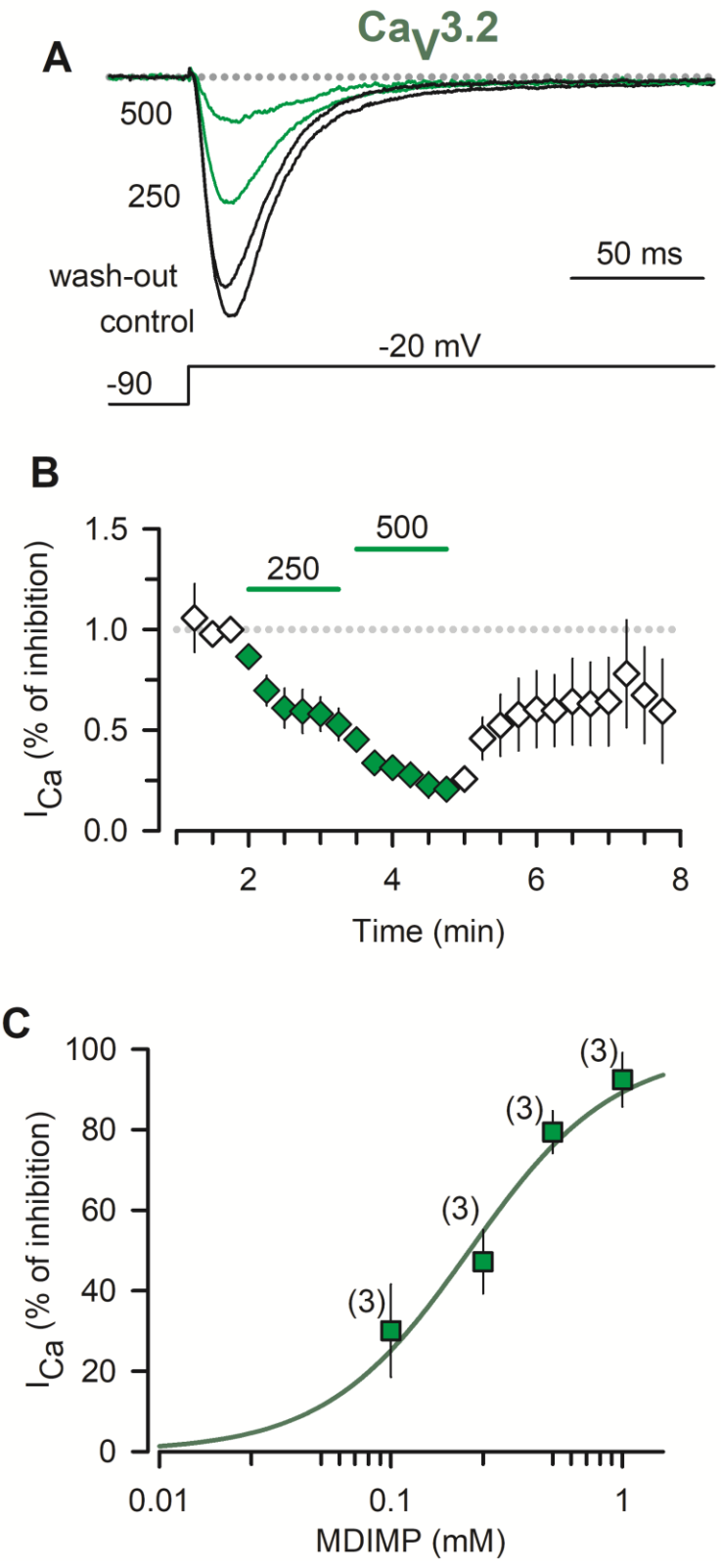

Molecular Pharmacology Fast Forward. Published on June 25, 2020 as DOI: 10.1124/mol.120.119982
This article has not been copyedited and formatted. The final version may differ from this version.

FIGURE 4

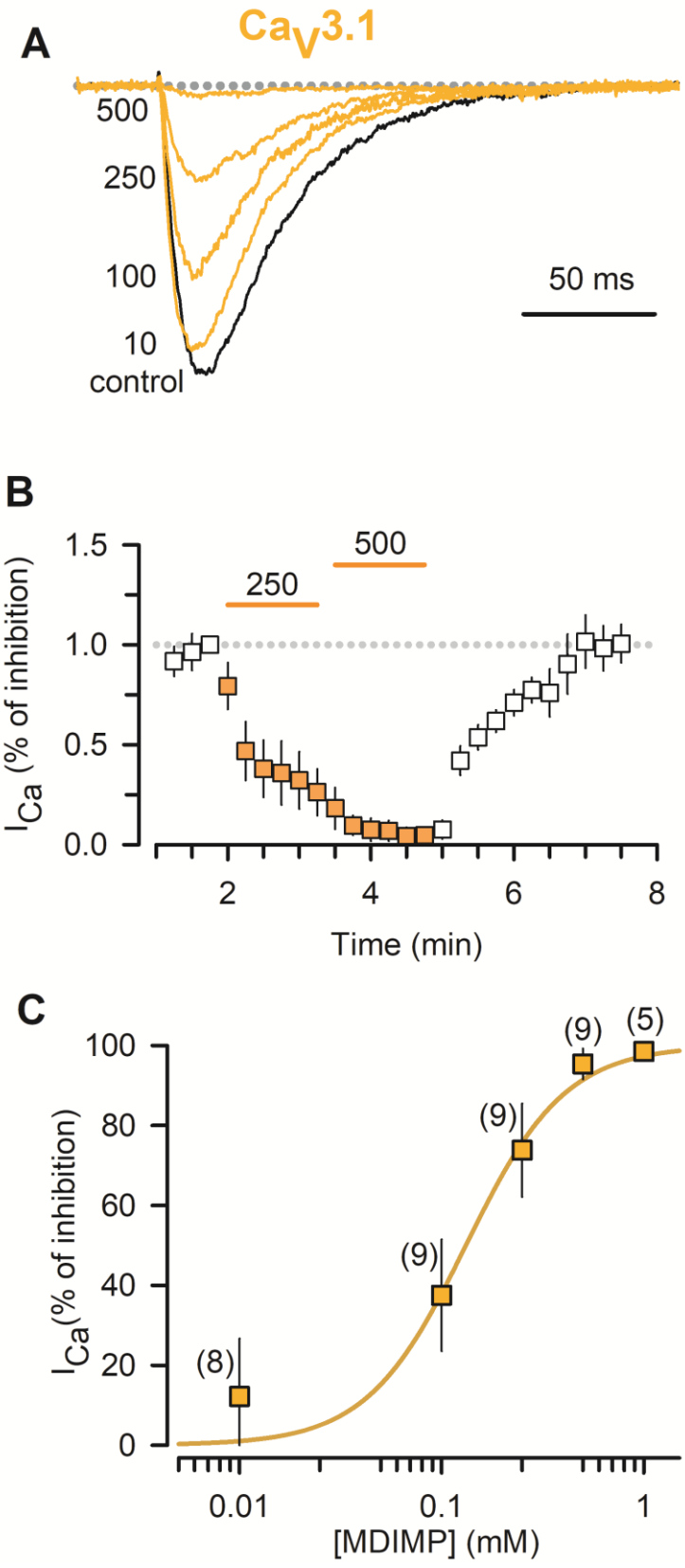

Molecular Pharmacology Fast Forward. Published on June 25, 2020 as DOI: 10.1124/mol.120.119982
This article has not been copyedited and formatted. The final version may differ from this version.

FIGURE 5

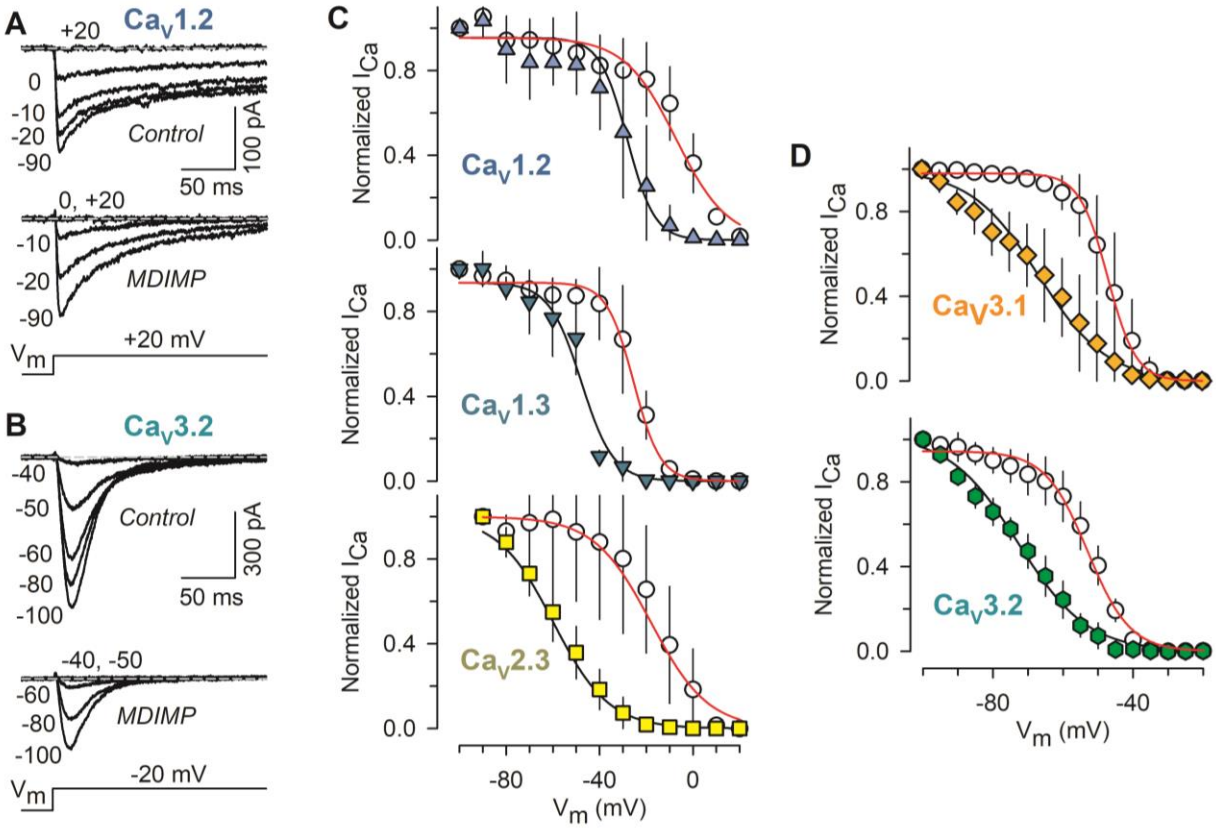

Molecular Pharmacology Fast Forward. Published on June 25, 2020 as DOI: 10.1124/mol.120.119982
This article has not been copyedited and formatted. The final version may differ from this version.

FIGURE 6

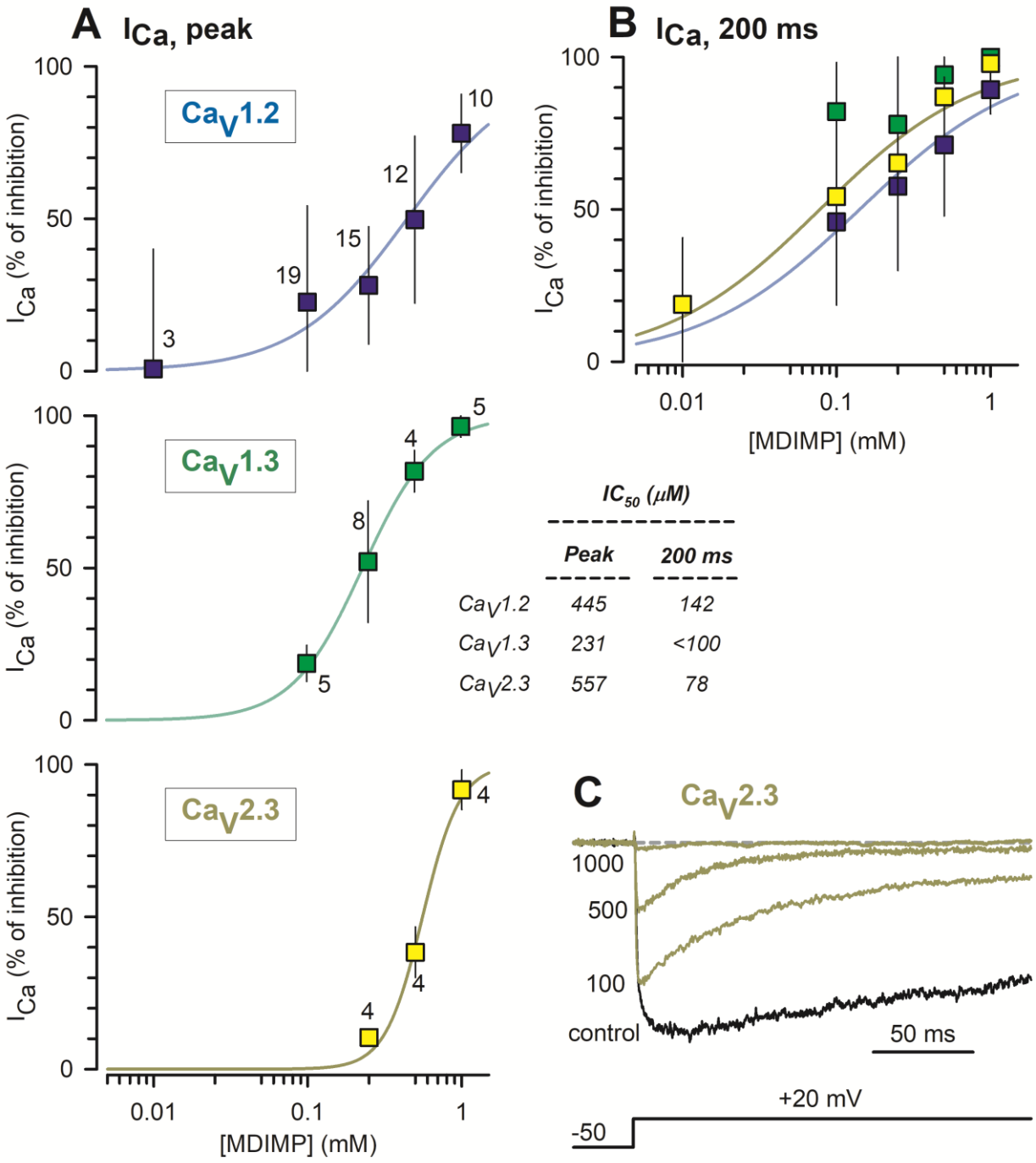

Molecular Pharmacology Fast Forward. Published on June 25, 2020 as DOI: 10.1124/mol.120.119982
This article has not been copyedited and formatted. The final version may differ from this version.

FIGURE 7

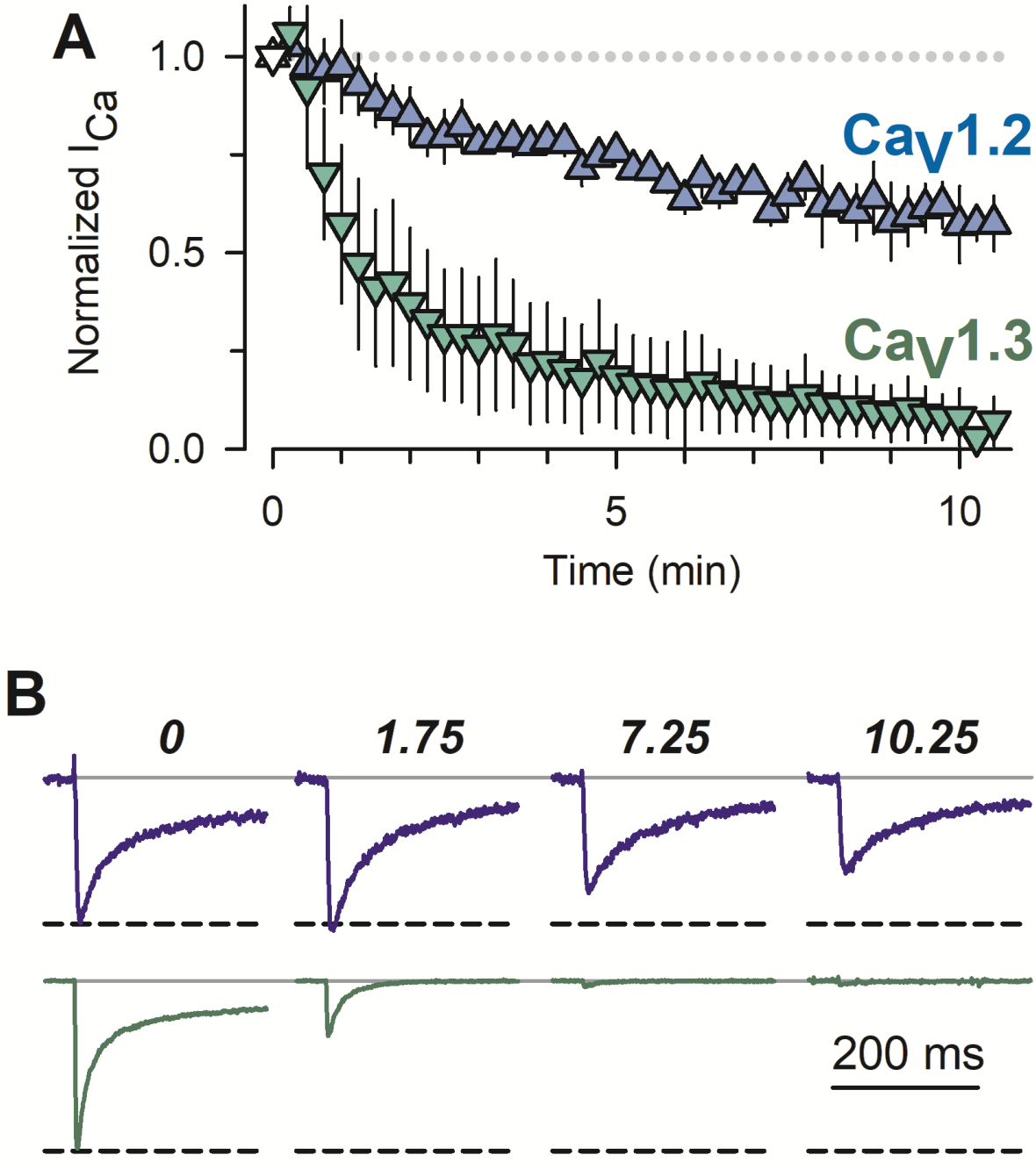

Molecular Pharmacology Fast Forward. Published on June 25, 2020 as DOI: 10.1124/mol.120.119982
This article has not been copyedited and formatted. The final version may differ from this version.

FIGURE 8

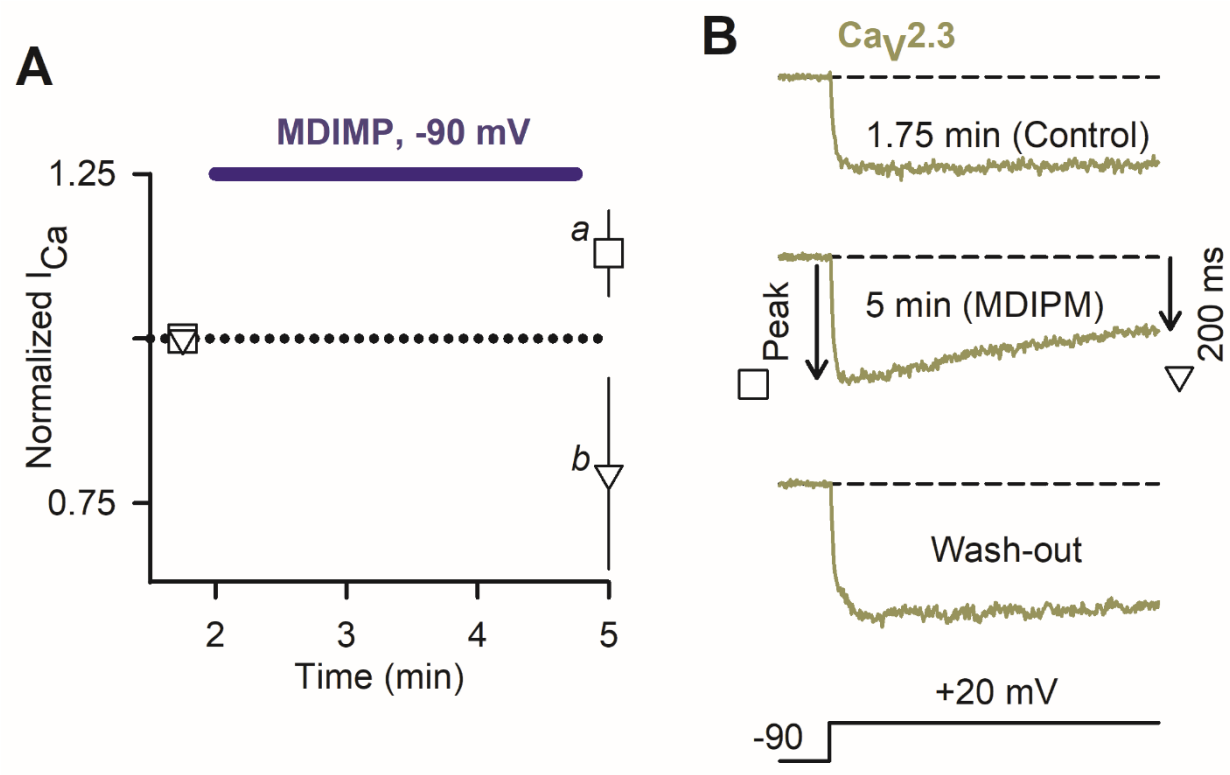

Molecular Pharmacology Fast Forward. Published on June 25, 2020 as DOI: 10.1124/mol.120.119982
This article has not been copyedited and formatted. The final version may differ from this version.

FIGURE 9

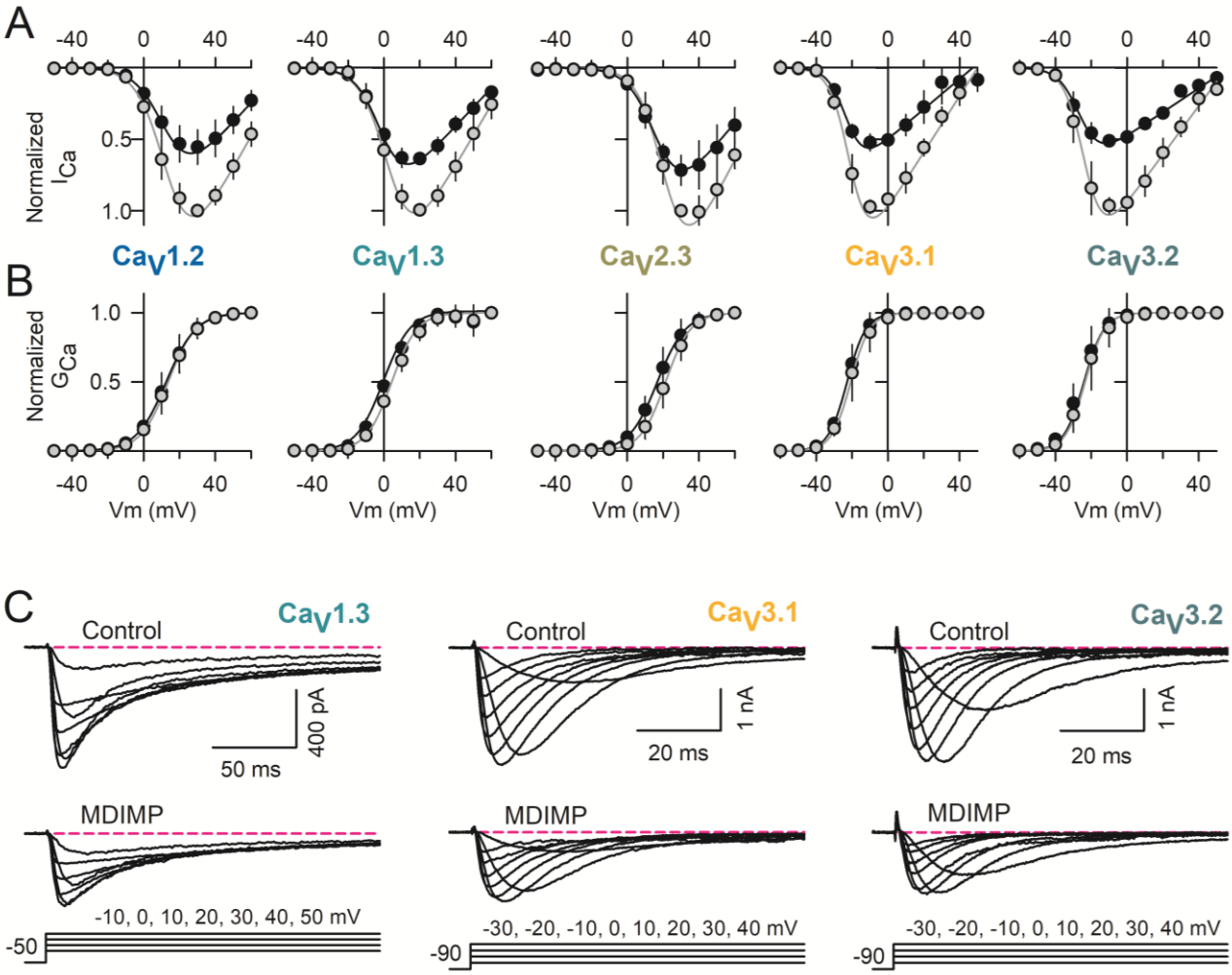

Molecular Pharmacology Fast Forward. Published on June 25, 2020 as DOI: 10.1124/mol.120.119982
This article has not been copyedited and formatted. The final version may differ from this version.

FIGURE 10

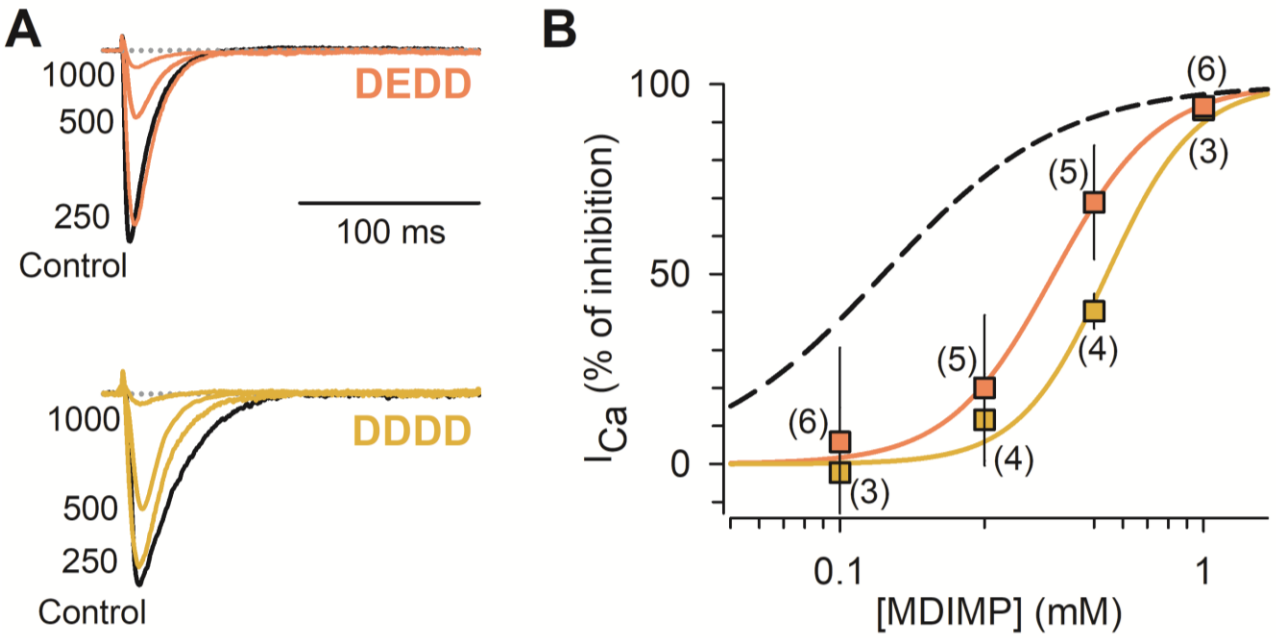

Molecular Pharmacology Fast Forward. Published on June 25, 2020 as DOI: 10.1124/mol.120.119982
This article has not been copyedited and formatted. The final version may differ from this version.

FIGURE 11

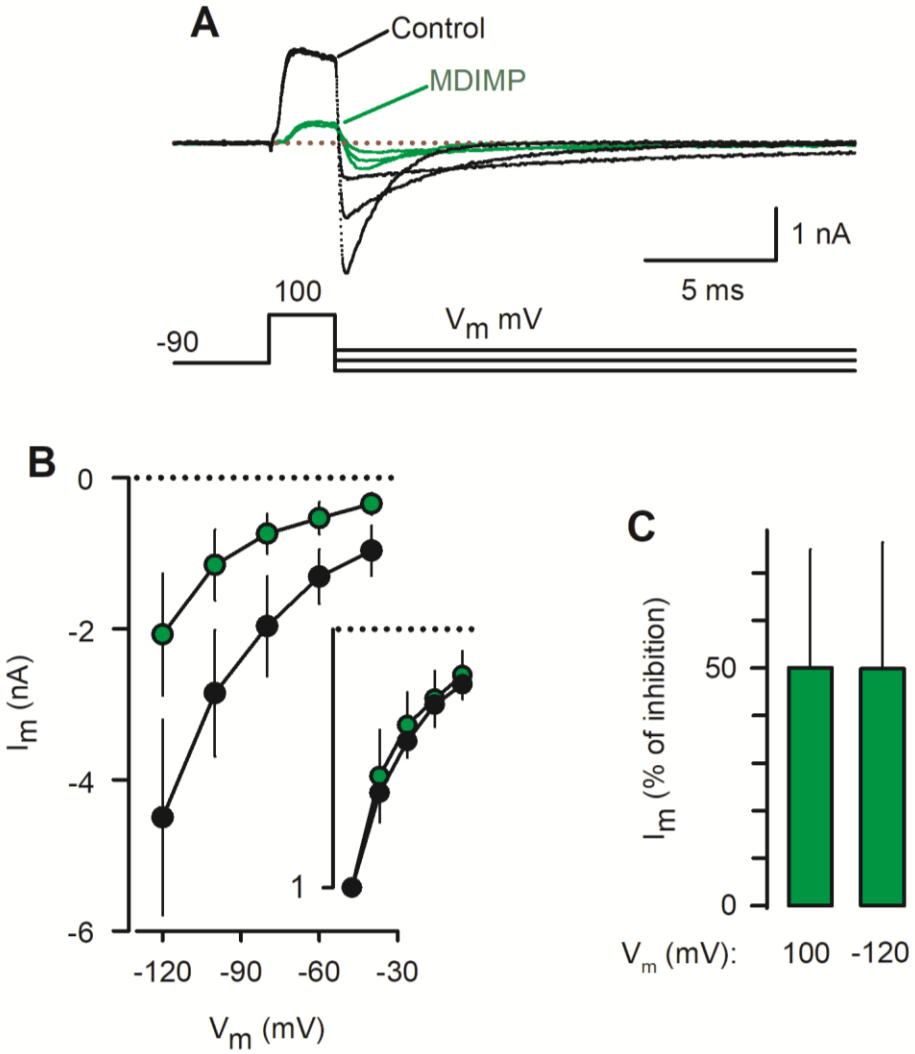

Supplementary Material

Interaction of MDIMP with the voltage-gated calcium channels

Juan A. M. De La Rosa[1], Maricela García-Castañeda[1], Takuya Nishigaki[2], Juan Carlos Gómora[3], Teresa Mancilla-Percino[4], and Guillermo Ávila[1,*]

Departamentos de Bioquímica[1] y Química[4], Cinvestav-IPN;

Institutos de Biotecnología[2] y Fisiología Celular[3], Universidad Nacional Autónoma de México.

* Corresponding author Guillermo Ávila, Ph.D.

gavila@cinvestav.mx

TABLE S-1

Parameters of fitted concentration-response curves

	HP = -90 mV					HP = -50 mV				
	n	I_{peak}		$I_{200\ ms}$		n	I_{peak}		$I_{200\ ms}$	
		IC_{50} (μM)	n_H	IC_{50} (μM)	n_H		IC_{50} (μM)	n_H	IC_{50} (μM)	n_H
$Ca_V1.2$	3-6	656	2.2	<250	*nd*	3-19	445	1.2	141	0.8
$Ca_V1.3$	2-6	957	3.5	290	2.9	4-8	231	1.9	<100	*nd*
$Ca_V2.3$	4-7	>1000	*nd*	717	4.6	3-7	557	3.6	78	0.9
$Ca_V3.2$	3	219	1.4							
$Ca_V3.1$	5-9	132	1.8							
$Ca_V3.1$ (DEDD)	4-6	387	3.0							
$Ca_V3.1$ (DDDD)	3-4	543	3.6							

nd, not determined.

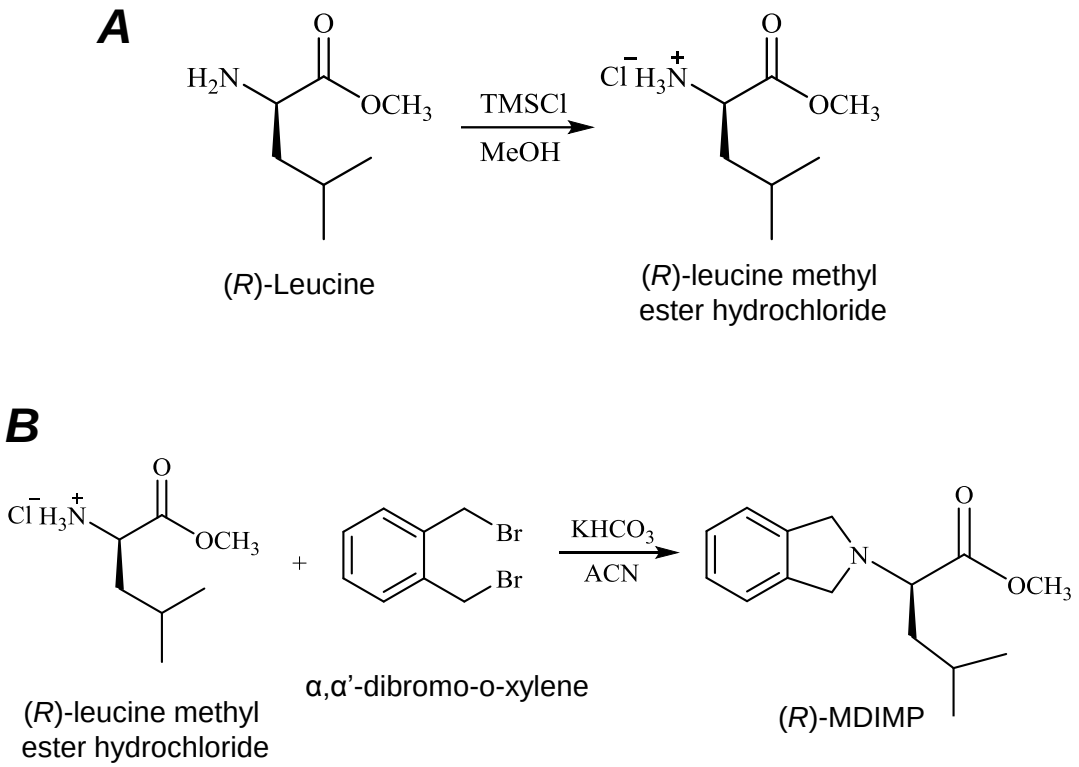

Figure S–1. Scheme depicting the approach to synthesize (*R*)-MDIMP (chemical name: methyl (*R*)-2-(1,3-dihydroisoindol-2-yl)-4-methylpentanoate). Chemical synthesis reagents were purchased from Sigma Aldrich Co®. ***A)*** The first step consisted in the preparation of (*R*)-leucine methyl ester hydrochloride under a nitrogen atmosphere as follow: in a 50 ml ball flask was placed 1.0 g (7.7 mmol) of (*R*)-Leucine, and then 1.94 ml (16 mmol, 2 equiv) of trimethylsilyl chloride (TMSCl) were slowly added. The reaction mixture was stirred at room temperature for 30 min, after this time, 8 ml of MeOH were added, and the reaction mixture was left again under agitation for 24 h. Next, the solvent was evaporated under reduced pressure, yielding 1.32 g (96 %) of (*R*)-leucine methyl ester hydrochloride (white solid, m.p.:150-152 ^{o}C). ***B)*** In a 250 ml ball flask were placed (*R*)-leucine methyl ester hydrochloride (344 mg, 1.89 mmol), $KHCO_3$ (570 mg, 5.69 mmol), α,α'-dibromo-o-xylene (500 mg, 1.89 mmol) and acetonitrile (60 ml), the suspension was refluxed for 6 h. After being cooled to room temperature under nitrogen atmosphere, the solution was filtered, and the solvent was removed under reduced pressure, and the remaining solid was treated with 20 mL of AcOEt and 10 mL distilled water and were carried out three extractions with AcOEt (20 mL), to the organic layer was added anhydrous sodium sulfate. The solution was filtered and the solvent was removed under reduced pressure to yield 400 mg of a solid, which was purified by silica gel chromatography (using a 9:1 mixture of chloroform and acetonitrile, as eluent). Yield 264 mg (50%) of (*R*)-MDIMP; m.p. 60-61^{o}C (Melting point was taken in open capillary tube on a Gallenkamp equipment). The structure of (*R*)-MDIMP was characterized by ^{1}H, ^{13}C NMR and high-resolution mass spectroscopy (HRMS). NMR spectra were recorded on JEOL ECA 500 spectrometer, chemical shifts are reported relative to TMS and $CDCl_3$ used as solvents. The spectrum of high-resolution mass was obtained on an Agilent Technologies Model LC/MSD-TOF spectrometer, coupled to HPLC 1100 with ESI as ionization source. ^{1}H NMR (500 MHz): δ 0.94 (d, $^{3}J_{HH}$ = 6.2 Hz, 3H, CH_3), 0.97 (d, $^{3}J_{HH}$ = 6.2 Hz, 3H, CH_3), 1.69-1.72 (m, 3H, C<u>H</u>$(CH_3)_2$ and C<u>H</u>$_2$-$CH(CH_3)_2$), 3.61 (t, $^{3}J_{HH}$ = 7.4 Hz, 1H, NC<u>H</u>CO), 3.69 (s, 3H, OCH_3), 4.07 and 4.20 (dd, $^{2}J_{HH}$ = 10.4 Hz, 4H, CH_2NCH_2) 7.18 (s, 4H, C_6<u>H</u>$_{4\ arom}$). ^{13}C NMR (125 MHz): δ 22.64 (CH_3), 22.78 (CH_3), 25.13 (<u>C</u>H$_2$-$CH(CH_3)_2$), 40.12 (<u>C</u>H$(CH_3)_2$, 51.36 (OCH_3), 55.21(CH_2NCH_2), 62.43 (N<u>C</u>HCO), 122.42, 126.73, 139.57 (<u>C</u>$_6$H$_4$) and 173.97 (C=O). HRMS-ESI: $C_{15}H_{22}NO_2$ $[M+H]^+$, calc. 248.1645 and found 248.1646.

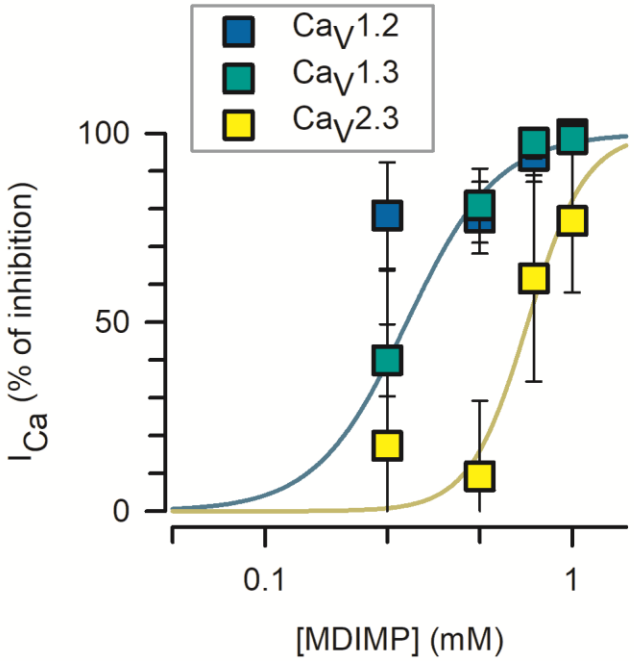

Figure S–2. Concentration-response curves for I_{Ca} carried through HVA Ca^{2+} channels, 200 ms after depolarization. The results were obtained using a HP of -90 mV, and are from the same data sets as those shown in figures 1 ($Ca_V1.2$ and $Ca_V1.3$) and 2 ($Ca_V2.3$). The IC_{50} values are given in both the text and Table S–1.

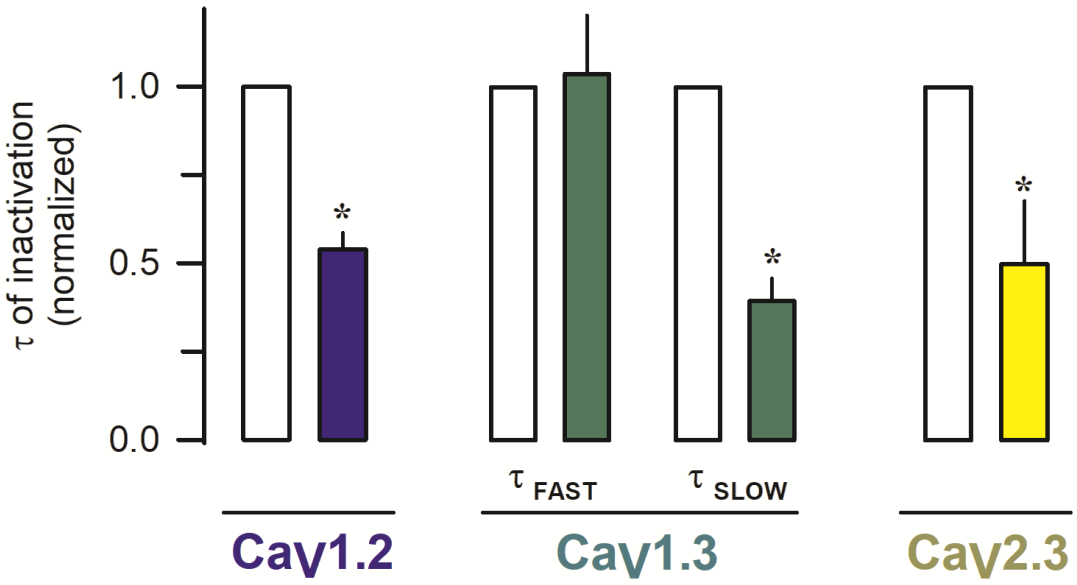

Figure S–3. The MDIMP accelerates the inactivation kinetics of HVA Ca^{2+} channels. The decaying phase of I_{Ca} was fitted according to a single ($Ca_V1.2$ & $Ca_V2.3$) or second ($Ca_V1.3$) order exponential equation. Then, for each cell, the resulting time constants (τ) were normalized relative to the corresponding control (open bars). The mean control values were (in ms): 62.3 ($Ca_V1.2$), 11.0 (τ_{FAST}), 85.3 (τ_{SLOW}), and 181.1 ($Ca_V2.3$). The results are from data shown in figures 1 and 2, and the colored bars indicate the presence of MDIMP (1 mM). *$p < 0.05$.

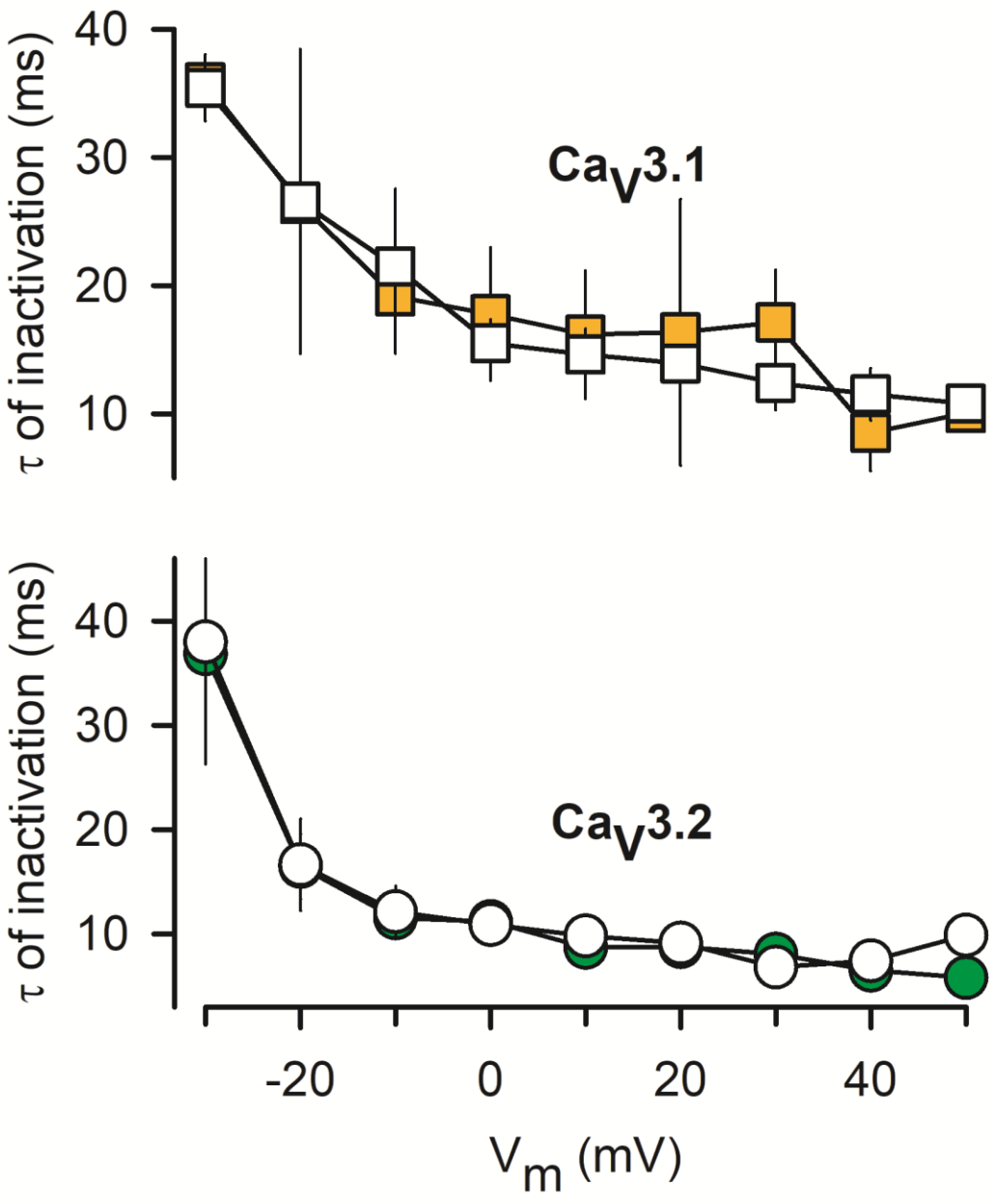

Figure S–4. MDIMP does not alter the inactivation kinetics of LVA Ca^{2+} channels. I_{Ca} was elicited as described in figures 3 and 4, but at distinct membrane potentials (V_m). The recordings were performed in the absence (open symbols) and presence of MDIMP (colored symbol), at concentrations close to the IC_{50} values obtained for each channel type 130 µM (colored squares) and 220 µM (colored circles). The time constant of inactivation (τ) was estimated by fitting the decaying phase of I_{Ca} to a single exponential equation. The results represent data obtained from four (squares) and three (circles) different cells.

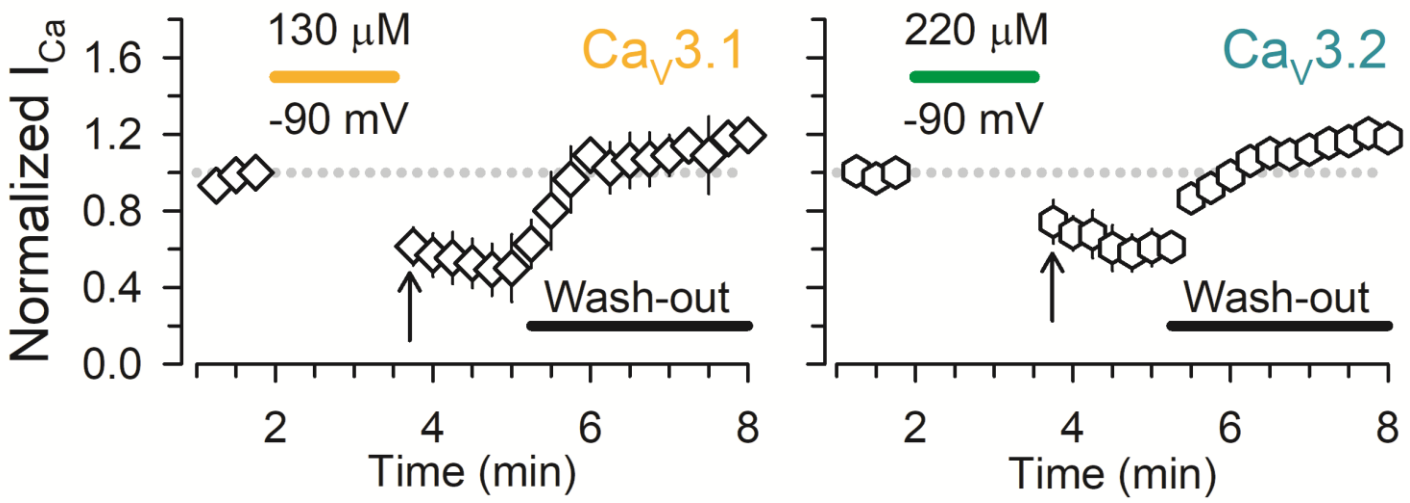

Figure S–5. MDIMP binds to the closed state of LVA Ca^{2+} channels. Normalized values of peak I_{Ca} that were obtained from cells expressing $Ca_V3.1$ and $Ca_V3.2$, before and two min after being exposed to MDIMP (130 µM and 220 µM). Test pulses to -20 mV were delivered from the HP (-90 mV), and the stimulation ceased during the MDIMP application (colored lines). Then, the stimulation was resumed (arrows), followed by an extensive wash-out of MDIMP. n = 6, for both $Ca_V3.1$ and $Ca_V3.2$.

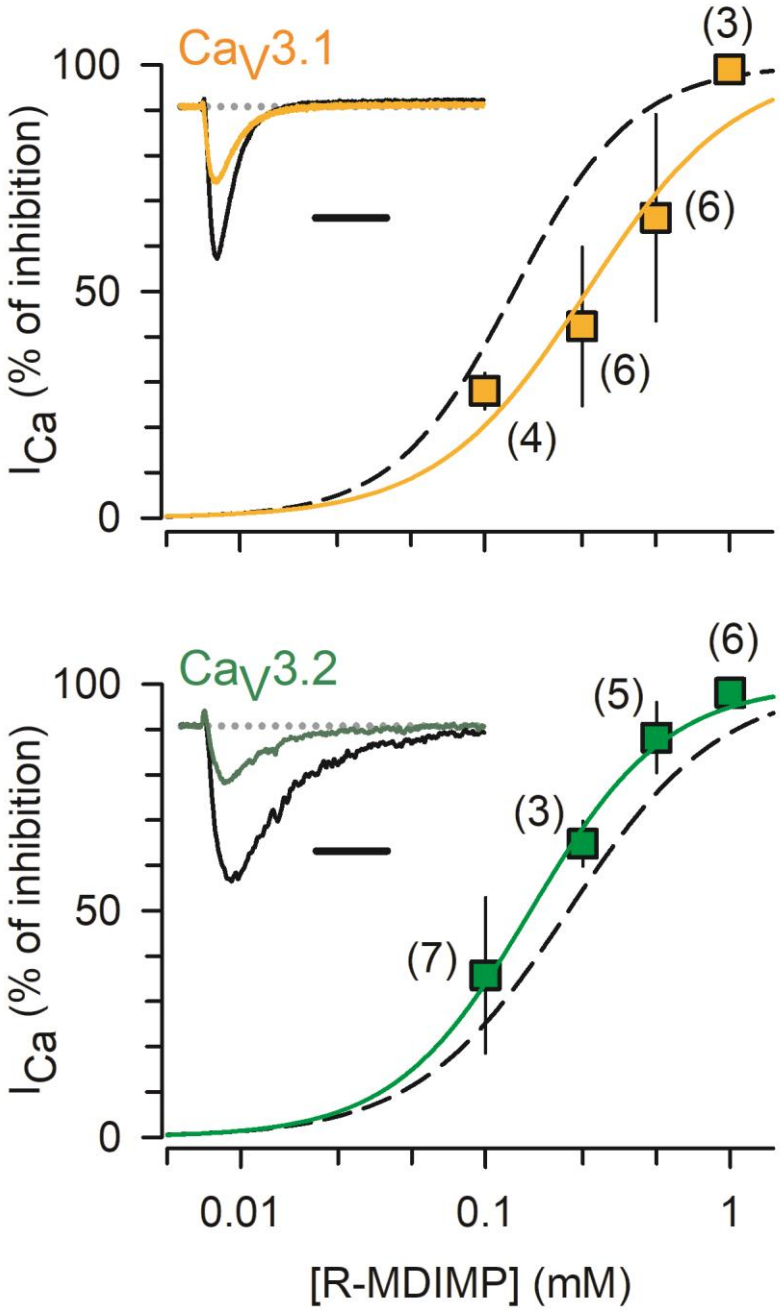

Figure S–6. The enantiomer of MDIMP [(*R*)-MDIMP] also inhibits Ca_V3 channels. Concentration-response curves for (*R*)-MDIMP effects on $Ca_V3.1$ and $Ca_V3.2$ channels. Ca^{2+} currents were converted to the percentage of inhibition and the corresponding average values were plotted as a function of the (*R*)-MDIMP concentration. The estimated IC_{50} and n_H values were: 261 µM and 1.4 ($Ca_V3.1$), and 153 µM and 1.6 ($Ca_V3.2$). The insets show examples of I_{Ca} recordings that were obtained in the absence (black traces) and the presence of 250 µM (*R*)-MDIMP (colored traces). The currents were elicited at -20 mV, from a HP of -90 mV. The horizontal calibration bars represent 50 ms. Data obtained for MDIMP are also shown for comparison (dashed lines, see Figs. 3B and 4B).